Journal of Applied Physics PERSPECTIVE scitation.org/journal/jap

Perspectives and opportunities with multisubband plasmonics

Cite as: J. Appl. Phys. **134**, 010901 (2023); doi: 10.1063/5.0152527
Submitted: 30 March 2023 · Accepted: 28 May 2023 ·
Published Online: 7 July 2023

M. Montes Bajo,[1] J.-M. Chauveau,[2] A. Vasanelli,[3] A. Delteil,[2] Y. Todorov,[3] C. Sirtori,[3] and A. Hierro[1,a)]

AFFILIATIONS

[1]ISOM, Universidad Politécnica de Madrid, Madrid, Spain
[2]Université Paris-Saclay, UVSQ, CNRS, GEMaC, 78000 Versailles, France
[3]Laboratoire de Physique de l'École Normale Supérieure, ENS, CNRS, Université Paris Cité, Sorbonne Université, F- 75005 Paris, France

[a)]**Author to whom correspondence should be addressed:** adrian.hierro@upm.es

ABSTRACT

In highly doped semiconductor quantum wells (QWs), electrons populate various energy states from different subbands and, therefore, several optical intersubband transitions (ISBTs) can occur simultaneously. Coulomb coupling between these ISBTs gathers the strength of all the individual transitions and concentrates all the oscillator strength in a single collective excitation: the multisubband plasmon (MSP). MSPs are an excellent platform for the study of collective and exotic effects in semiconductors and for the demonstration of novel device concepts. Indeed, the high electronic densities involved in the collective excitation greatly enhance the coupling strength and enable the ultra-strong coupling regime between MSPs and either optical modes in a cavity or phonons in the semiconductor. In this Perspectives paper, after addressing the basic physics of MSPs and the state of the art, we outline the most promising paths for the research community in this topic from the point of view of basic physics, material platforms, and applications of MSPs.

I. INTRODUCTION

Intersubband transitions (ISBTs) are optical transitions between confined energy levels in a two-dimensional electron system, such as a quantum well (QW).[1] They have been the subject of research and study for decades,[1,2] due to both their interest as a platform for fundamental physics and materials studies, and their relevance in optoelectronic devices.[3,4] ISBTs were first observed in the seventies and eighties of the last century in the accumulation layer of n-Si in metal-oxide-semiconductor structures[5] and inversion layers in GaAs/AlGaAs heterostructures.[6] In 1985, ISBTs were first observed by absorption spectroscopy in a GaAs/AlGaAs QW.[7] Current epitaxial growth techniques, such as molecular beam epitaxy (MBE) or metal-organic chemical vapor deposition (MOCVD), allow the growth of semiconductor heterostructures with excellent interfacial quality, which fuels the research attention toward ISBTs.

QWs made from well-known and mature optoelectronic semiconductors—such as those from the GaAs or InP families—can feature ISBTs from the near infrared (IR) to the THz range of the electromagnetic spectrum. Therefore, ISBTs are at the core of technological applications, such as quantum well infrared photodetectors (QWIPs),[3] quantum cascade detectors (QCDs),[8] and quantum cascade lasers (QCLs),[4,9,10] which operate in the mentioned frequency ranges.

If the confined levels in the QW are closely spaced together and/or several of them are populated by electrons, several ISBTs can happen simultaneously. Counterintuitively, the optical response of such a system is not the appearance of a collection of spectral features corresponding to all the possible transitions, but only one spectral feature that collects all the strength of the individual transitions and does not match their individual frequencies. This phenomenon is called a multisubband plasmon (MSP)[11–13] and it is the subject of this perspectives paper.

MSPs have been the subject of intense research in the last decade[11–23] and have proven to be an excellent platform to investigate ultrastrong coupling of light and matter excitations in an optical cavity. Also, MSPs have been a system of choice for the

demonstration of superradiance,[20] a phenomenon by which an ensemble of excited electrons emits radiation collectively. MSPs, by their own nature, are ideally suited for this. More recently, MSPs have opened the field of semiconductor quantum plasmonics, where the plasmonic properties of a semiconductor structure can be controlled and tuned by the quantum confinement of the electrons in the materials, allowing for the development of quantum-controlled metamaterials.[14,22]

This perspectives paper aims to review the physics and state of the art of research in MSPs, and to outlook the next steps the research community is likely to follow in this topic. We begin (Sec. II) by describing the phenomenon of MSPs in semiconductor QWs, starting from the description of the physics of ISBTs and the concepts of depolarization shift and ISB plasmons, extending then the explanation to the case of multiple populated levels in the QWs and MSPs. We finish the section by describing the evolution of MSPs when the QWs get thick enough, and how they become confined 3D plasmons eventually reaching the regime of Berreman modes.

MSPs are also perfectly suited to couple to lattice vibrations, i.e., phonons, to generate a type of hybrid quasiparticle, the MSP polaron, whose characteristics are described in Sec. III.

Next (Sec. IV), we delve into the coupling of MSPs and photons in an optical cavity, where the ultra-strong coupling regime can be reached, owing in part to the large electron densities in the QWs producing the MSPs, and we describe the advantages of the capability of MSPs to be tuned via quantum confinement.

In Sec. V, we provide an overview of the different material platforms, both readily available and future, where MSPs can be excited and exploited for a variety of applications. We explore how material features such as dielectric constant, electron effective mass, or maximum attainable electron density impact their suitability for MSP-based studies and applications.

Finally, Secs. VI and VII are devoted to topics and applications to which we believe the MSP field is going to focus its attention, including ultrastrong coupling, superradiance, devices, and quantum plasmonics.

II. FROM INTERSUBBAND TRANSITIONS TO CONFINED 3D PLASMONS

A. Intersubband transitions

We begin by setting the basis of the concept of ISBTs between confined energy levels in a semiconductor QW. The reader is referred to the literature for a more in-depth discussion of the physics involved.[1–3]

A semiconductor QW consists of a thin layer (a few nm thick) of a semiconductor with a certain bandgap sandwiched between layers of another semiconductor with a larger bandgap. Examples of this are GaAs layers embedded in $Al_xGa_{1-x}As$ barrier layers or GaN layers in $Al_xGa_{1-x}N$, to name a few.

Solving the Schrödinger equation in this system yields the appearance of confined energy levels in the QW layer, as opposed to the continuous conduction and valence energy bands of the bulk semiconductor (Fig. 1, ISBT column). ISBTs are electronic transitions between confined levels in the QW. In this perspectives paper, we will illustrate all these phenomena with conduction band examples.

In the QW, an electron residing in the fundamental level can be promoted to the first excited level by the absorption of an incident electromagnetic wave with an energy equal to the energy difference between the levels, $\hbar\omega_{ISBT}$. The selection rules for intersubband absorption dictate that only the component of the electric field perpendicular to the QW plane can produce such a transition. Therefore, all optical experiments to probe these material excitations involve p-polarized light (i.e., transverse magnetic—TM—polarization). The intensity of the ISBTs between electronic levels depends on the oscillator strength, f_{ISBT}, between the energy levels involved. Due to considerations about the respective parity of the wavefunctions corresponding to the levels involved, the oscillator strength is non-negligible only for transitions between states with opposite parity. Hence, only transitions from level 1 to levels 2, 4 etc., in the QW—if they are available—are allowed, whereas transitions from level 1 to levels 3, 5 etc., are forbidden. The same applies to transitions from a higher to lower energy level. It is worth mentioning that the oscillator strength has the largest values for transitions between adjacent energy levels. Therefore, ISBTs between adjacent levels dominate.[1]

The interaction of light with an ISBT is usually described in the semiclassical limit via an anisotropic dielectric function, in which the in-plane response of the materials is described with the Drude model and the out-of-plane component features a Lorentzian resonance centered in the frequency of the ISBTs:[1–3]

$$\varepsilon_{in\ plane} = \varepsilon_\infty - \frac{\omega_{p||}^2}{\omega^2 + i\gamma_{||}\omega}, \tag{1a}$$

$$\varepsilon_{out\ of\ plane} = \varepsilon_\infty + \frac{\omega_p^2}{\omega_{ISBT}^2 - \omega^2 - i\gamma\omega}. \tag{1b}$$

In Eq. (1a), ε_∞ is the high frequency dielectric constant, $\omega_{p||}^2 = e^2\Delta n_{2D}/(m^*\varepsilon_0\varepsilon_\infty L)$ is the in-plane plasma frequency with a broadening given by $\gamma_{||}$, L is the thickness of the doped region, e is the elementary charge, and ε_0 is the permittivity of vacuum. In Eq. (1b), ω_{ISBT} is the frequency at which the ISBT is centered and $\omega_p^2 = f_{ISBT}e^2\Delta n_{2D}/(m^*\varepsilon_0\varepsilon_\infty L_{eff})$ is the screened plasma frequency of the ISBT with a broadening given by γ. In this expression, Δn_{2D} is the difference in two-dimensional electron density between the levels involved in the ISBT and L_{eff} is the effective length over which the ISBT takes place.[2,24] Figure 1 (ISBT column) illustrates how the ISBT can be observed optically at the frequency where the imaginary part of $\varepsilon_{out\ of\ plane}$ (i.e., the loss function) has a maximum.

B. Intersubband plasmons

In a doped QW structure, there is not only one single electron in the fundamental level of the QW but a certain density of conduction electrons [Fig. 1(a), ISBP column]. In this case, upon illumination of the structure with light of the appropriate energy and polarization, the electrons experience a collective excitation due to the electromagnetic wave, known as intersubband plasmon (ISBP).

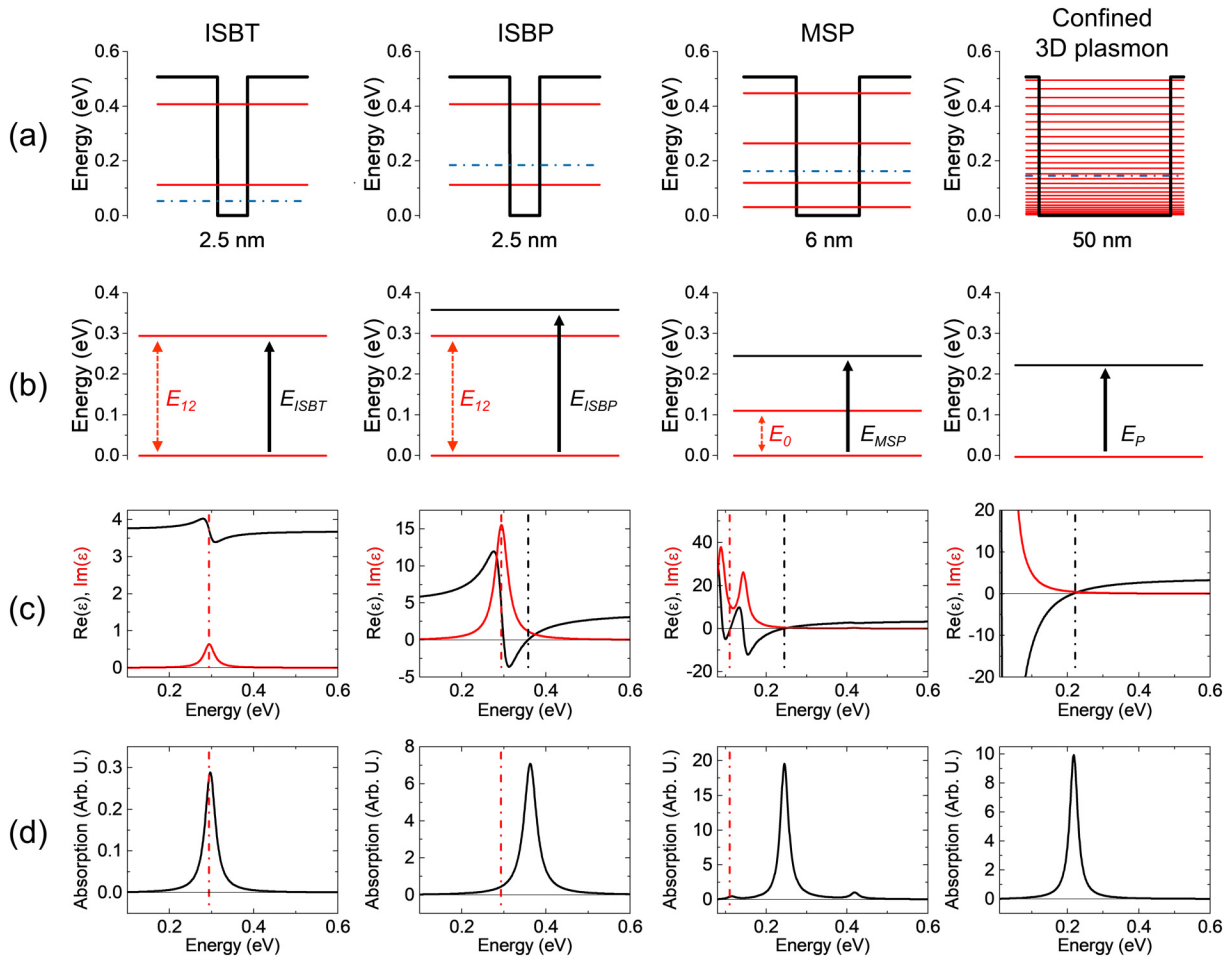

FIG. 1. Energy diagram in the real space (a), intersubband and plasmonic excitations (b), real and imaginary parts of the out-of-plane dielectric function (c), and absorption spectrum (d), for all the phenomena described in this section: ISBT of a single electron, ISBP where a density of electrons is involved, MSP, when several ISBPs occur simultaneously, and 3D confined plasmons or Berreman modes, where the energy levels in the QW are closely spaced together and the optical excitation takes place at the plasma energy. Blue, dashed-dotted line in (a) is the Fermi energy. Vertical red, dashed lines in (c) and (d) represent the energy of the bare ISBT or multisubband excitation, without considering plasma effects (i.e., E_{12} for ISBP or E_0 for MSP). Vertical black dashed lines in (c) represent the actual energy at which the excitation takes place. All calculations performed for a $Zn_{0.7}Mg_{0.3}O/ZnO$ QW.

This collective excitation results in the renormalization of the transition energy, which is not observed at the energy of the bare ISBT, $\hbar\omega_{ISBT}$, but at a higher energy given by $E_{ISBP} = \hbar\sqrt{\omega_{ISBT}^2 + \omega_p^2}$. This energy corresponds to the higher-energy root of Eq. (1b) [Figs. 1(c) and 1(d), ISBP column], therefore in essence, this phenomenon is akin to an epsilon-near-zero (ENZ) mode.[25,26] This increase in the resonance energy of the ISBP with respect to the ISBT is known as *depolarization shift*, and it gets stronger as the 2D electron concentration in the QW increases due to the dependence $\omega_p \propto \sqrt{n_{2D}}$.[1,2]

C. Multisubband plasmons

In more general terms and allowing for the possibility that there are more than two confined levels in the QW (Fig. 1, MSP column), the plasma frequency for each transition between two levels is given by $\omega_{p,i} = \sqrt{\frac{\Delta n_{2D,i} f_i e^2}{m^* \varepsilon_0 \varepsilon_\infty L_{eff,i}}}$, where the subindex i is a label for each allowed transition, $\Delta n_{2D,i}$ is the difference in two-dimensional electron density between the two levels involved in the transition, $L_{eff,i}$ is the ISBT effective length, and f_i is the oscillator strength for each transition. This expression assumes the effective mass is the same for each subband. Nonparabolicity of the bands is not considered in this expression, although it has been addressed in the literature.[16]

In this situation, one could expect the appearance of a series of ISBPs, each corresponding to an allowed transition between a pair of levels, depolarization-shifted according to each value of $\omega_{p,i}$, and weighted in intensity according to the relative electron population of the two levels involved in each case. However, a strikingly different phenomenon takes place.

Early reports predicted that if the depolarization-shifted transition between the first two levels increases its energy due to the increase in electron density until it resonates with the next allowed transition, the evolution of both resonances' energies and intensities is modified by the coupling between the two original excitations.[27] Later, Li *et al.*[28] predicted that a transparency phenomenon is induced in this case: the transition between the two first levels essentially vanishes, whereas the high energy one "captures" all the intensity of both transitions and keeps shifting to higher energy with increasing n_{2D} (Fig. 2).

Later, Delteil *et al.*[11] reported both theoretically and experimentally on the coherence between ISBPs in a QW, mediated by Coulomb interaction. In this paper, the predictions from Li *et al.*[28] are extended to a system with more than two interacting ISBPs. It is shown that the absorption spectrum from a doped, 18.5 nm-wide GaInAs/AlInAs QW, from which up to four independent ISBPs from four pairs of levels were expected, feature only one strong peak at an energy that does not match that of any of the individual transitions. This resonance was named a bright multisubband plasmon (MSP).

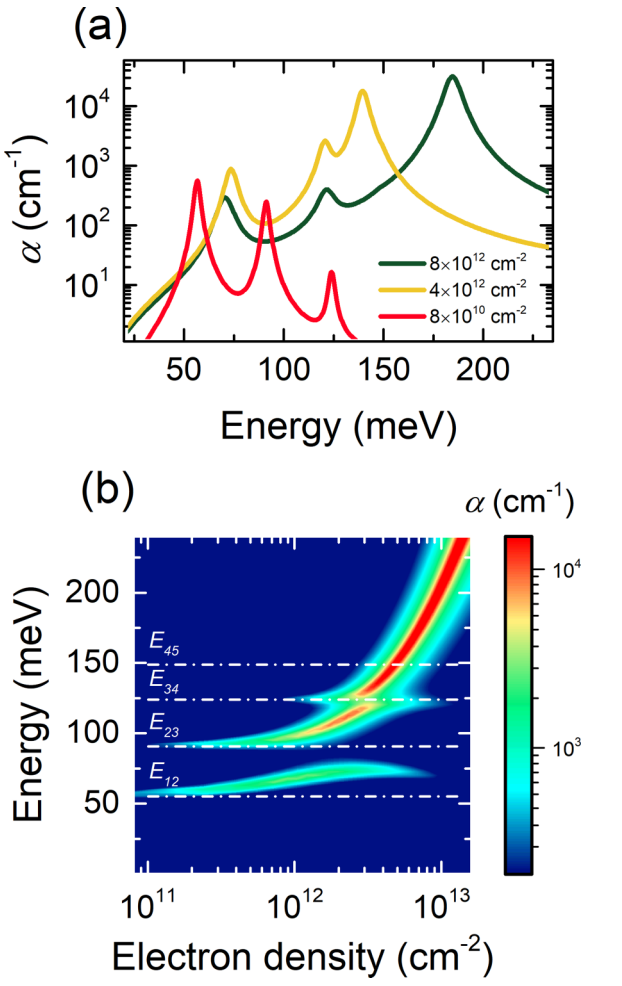

FIG. 2. (a) Absorption coefficient for a 8 nm-thick 30% Mg ZnO/ZnMgO QW with various electron concentrations at RT. (b) Color map showing the absorption coefficient of said QW as a function of the 2D electron concentration. The energies of the bare 1 → 2, 2 → 3, 3 → 4, and 4 → 5 ISBTs are indicated.

The out-of-plane electromagnetic response of such a system can be described by the sum of all the Lorenztian oscillators corresponding to each individual transition involved,

$$\varepsilon(\omega) = \varepsilon_\infty + \sum_i \frac{\omega_{p,i}^2}{\omega_i^2 - \omega^2 - i\gamma_i\omega}. \tag{2}$$

It is shown[11–13] that, in the case of a square quantum well, the MSP can also be likened to a single ISBP between two virtual levels, with energy E_0, and an effective plasma energy related to the plasma energies of the non-interacting individual ISBPs, E_P, such that

$$E_P = \hbar\Omega_p = \sqrt{\sum_i \hbar^2\omega_{p,i}^2}, \tag{3a}$$

$$\frac{1}{E_0^2} = \frac{1}{\hbar^2}\frac{1}{\sum_i \omega_{p,i}^2}\sum_i \frac{\omega_{p,i}^2}{\omega_{ISBT,i}^2}., \tag{3b}$$

and the resonance appears experimentally at a depolarization-shifted energy of

$$E_{MSP} = \sqrt{E_0^2 + E_P^2}. \tag{4}$$

D. Confined 3D plasmons

If the QW is widened even further so the confined levels get closely spaced in energy, while maintaining or increasing the electron density in the QW, an increasing number of levels become populated (Fig. 1, confined 3D plasmon column). From Eqs. (3) and (4), it can be seen that in this case E_0 becomes small and E_{MSP} becomes closer to E_P, while still retaining some controllability of the phenomenon via the quantum confinement. In this situation, the phenomenon gets closer to a 3D bulk plasmon in a subwavelength layer, sometimes called Berreman mode.

III. ULTRASTRONG COUPLING OF MSPs TO PHONONS

The lattice vibrations in a material, phonons, can be portrayed as harmonic oscillators, which can interact and couple to other material excitations with similar energy. In the case of polar materials, both transverse (TO) and longitudinal (LO) optical phonons appear, whose oscillator energies lie in the mid- to far-infrared, sharing the electromagnetic spectrum with ISBTs and MSPs. As discussed in Sec. V, the energy of the TO and LO phonons ($E_{TO} = \hbar\omega_{TO}$ and $E_{LO} = \hbar\omega_{LO}$, respectively) of the most common semiconductors covers the range from 15 to 100 meV.

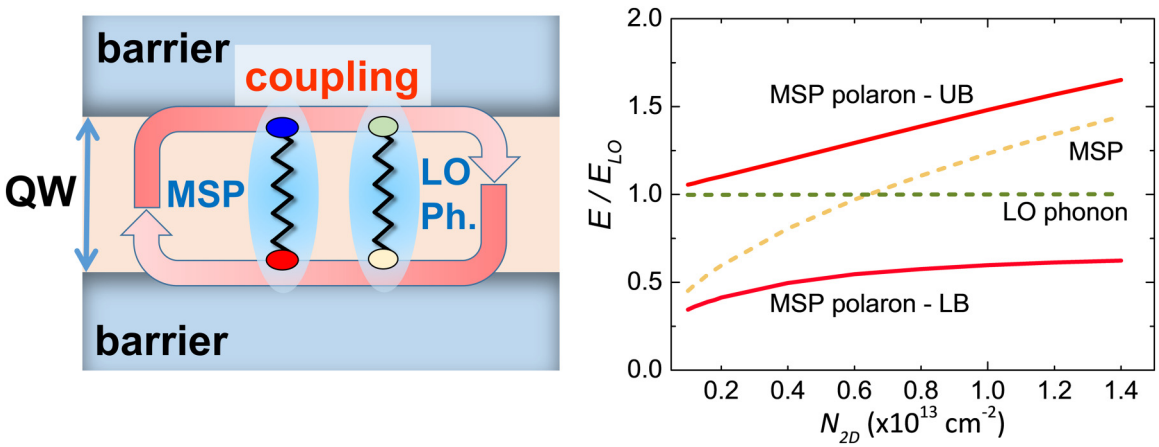

FIG. 3. (Left) Scheme of a quantum well where the MSP and LO phonon oscillator are coupled to form a MSP polaron. (Right) MSP polaron dispersion curves as a function of the 2D electron concentration that results from coupling between the MSP and the LO phonon. UB/LB refers to the upper/lower branch.

The interaction of these LO phonons with electrons in a polarizable medium leads to a quasi-particle labeled polaron, already described in the first half of the 20th century. However, the coupling of ISBPs to LO phonons was much more recently described[29–31] with a microscopic model finally developed by De Liberato and Ciuti.[32] This microscopic theory was later generalized to the case of a MSP by Ribeiro *et al.*,[15] where the formalism for the MSPs earlier developed by the group,[11,33] which accounted for Coulomb electron–electron interactions, was extended to include phonon–electron Fröhlich interactions. In analogy to the case of polarons, the quasi-particle arising from the coupling between the ISBT/MSP and the LO-phonon is labeled intersubband/MSP polaron (Fig. 3, left panel).

It is interesting to note that, in most optoelectronic applications, one tries to avoid the spectral region where the phonons are found. Indeed, phonons show very strong reflectance across the entire frequency range between ω_{TO} and ω_{LO}, a region that is known as the reststrahlen band. However, it is precisely the frequency range where the coupling with a MSP can take place, which can easily reach the ultrastrong regime, leading to a rich ensemble of physical phenomena such as non-linear polariton splitting,[34] quantum phase transitions,[35] or quantum vacuum emission.[36] Of all examples where phonons are coupled to ISBTs in a device, QCLs clearly stand out.[9] In these lasers, population inversion is controlled via scattering with an LO-phonon. Indeed, coupling the ISBT between two confined energy levels with an LO-phonon allows to achieve very low electron lifetimes in the ground level.[37]

From the microscopic quantum theory of intersubband and MSP polarons,[15,32] one can prove that, in the semi-classical limit, the strength of the coupling between MSPs and phonons, Θ_{MSP}, is proportional to

$$\Theta_{MSP} \propto \sqrt{\frac{n_{2D}E_{LO}}{\varepsilon_\rho m^*}\frac{\mathrm{E}_0}{\mathrm{E}_{MSP}}}, \tag{5}$$

where n_{2D} is the two-dimensional electron density in the quantum well, and $\varepsilon_\rho = 1/\left(\frac{1}{\varepsilon_\infty} - \frac{1}{\varepsilon(0)}\right)$ is the reduced dielectric constant, with ε_∞ and $\varepsilon(0)$ being the high-frequency and static dielectric constants, respectively. The reduced dielectric constant is a measure of how different ε_∞ and $\varepsilon(0)$ are, and it has a small value when the $\varepsilon_\infty - \varepsilon(0)$ difference is large. By using the Lydanne–Sachs–Teller relation,[38] it can be readily shown that this is equivalent to the case of having a material with a very large $\omega_{LO} - \omega_{TO}$ difference, i.e., a very wide reststrahlen band. In Eq. (5), it is clear that, in order to increase the coupling strength between phonons and MSPs, both a high 2D electron concentration and LO-phonon energy are desired, together with a small electron effective mass and a low reduced dielectric constant, i.e., with a wide reststrahlen band.

As shown in Refs. 32 and 15, the coupling strength between phonons and MSPs is maximum when the MSP energy matches the phonon energy, i.e., when $\mathrm{E}_{MSP} = E_{LO}$. This coupling yields two MSP polaron branches (Fig. 3, right panel) with a mixed phononic–plasmonic character. At electron densities below the crossing point between the phonon and MSP energies, the lower polaron branch retains a plasmonic character, and becomes more phononic as the quantum well concentration is increased. In contrast, the upper polaron branch retains the phononic character below the $\mathrm{E}_{MSP} = E_{LO}$ crossing point, and becomes heavily plasmonic-like for high electron concentrations. Finally, at the electron concentration at which the $\mathrm{E}_{MSP} = E_{LO}$ condition is met, both branches of the MSP polaron mixed state are equally plasmonic and phononic in character, and the maximum coupling is achieved.

One of the remarkable features about the MSP polaron is that very large coupling energies can be achieved, comparable to the bare energy of the excitation (E_{LO}), hence reaching the ultra-strong coupling regime. It is insightful to note that, as indicated by De Liberato and Ciuti,[32] these very large coupling strengths arise from the superradiant nature of the ISBPs/MSPs, as well as from the very small volume of the phonon mode, which is highly confined within the quantum well. Indeed, the coupling strength in Eq. (5) scales as

$\sqrt{n_{2D}}$ and does not depend on the number of quantum wells, implying that increasing the number of quantum wells will not increase the coupling. Hence, highly polar materials with a very wide reststrahlen band and where very high dopings can be achieved will yield very high couplings. In this context, ZnO MSPs[21] are particularly interesting, as they display a huge coupling strength with optical phonons that can reach close to 40% of the MSP energy. This value can be further increased if more than two subbands are occupied, where couplings above 50% can be achieved. Overall, MSP polarons offer very high couplings, but have been scarcely used, hence the possibilities in this field are wide open. In Sec. V, we discuss some of the most interesting materials platforms that could serve to fully exploit MSP polarons.

Before concluding this section, we would like to mention that collective electronic excitations also play an important role in another class of mid-infrared lasers, the so-called intersubband Raman lasers,[29] where lasing is mediated by coupled ISBP–LO phonon modes. These devices are based on a double quantum well structure, with three confined electronic states. The ground state is populated, with electronic density N_g. A laser excites the intersubband plasmon 1–3, while the energy separation 1–2 is designed to be close to that of a LO-phonon. The Raman gain depends on the electronic density N_g.[39] As a consequence, in order to increase the gain, it could be interesting to investigate if Raman lasing can take place in the presence of coupled MSP–phonon modes.

IV. ULTRASTRONG COUPLING OF MSPs TO OPTICAL CAVITIES

In an equivalent way to the case of MSP polarons, when a MSP is coupled with an optical cavity mode [Fig. 4(a)], a unique regime of light–matter interaction is achieved: the ultra-strong coupling regime, characterized by a coupling energy (the Rabi energy, E_R) in the same order of magnitude as that of the matter excitation, given by the MSP energy.[40] In this regime, the quadratic and anti-resonant terms of the light–matter interaction cannot be neglected, as it is usually done in the weak and strong coupling regimes. These terms are the essential ingredients to produce peculiar quantum phenomena, like dynamical Casimir effect, superradiant phase transitions, modified photon blockade, extraordinary conductance, and cavity-assisted chemical and thermodynamic effects.[41,42]

The light–matter interaction between ISBPs and an optical mode yields a mixed state labeled intersubband polariton, which was initially described by Dini *et al.*[43] using an optical cavity

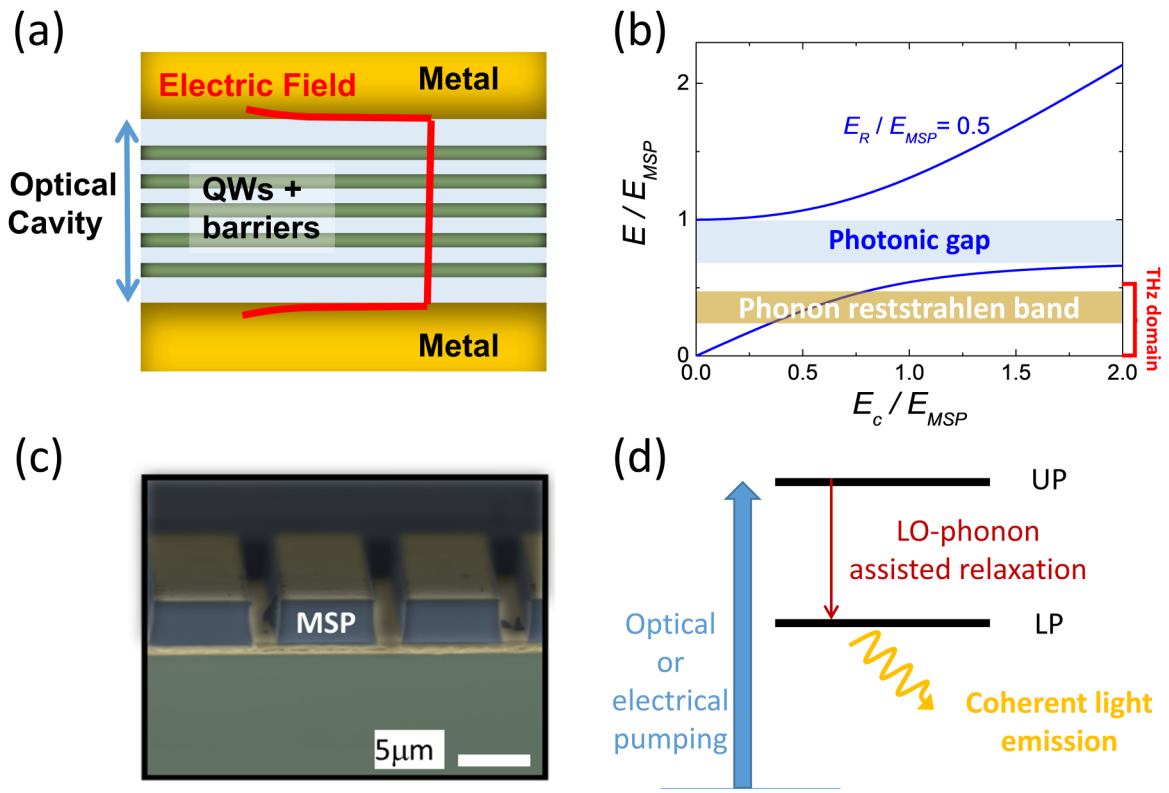

FIG. 4. (a) Schematic of a metal–insulator–metal optical microcavity filled with quantum wells. The electric field for a TM_0 mode is also shown. (b) MSP polariton dispersion as a function of the microcavity energy (E_c). Both axes are normalized by the uncoupled MSP energy (E_{MSP}). (c) Scanning electron microscope image of a double metal cavity, as the one sketched in panel (a). (d) Sketch of the operation of a laser based on the bosonic stimulation of multisubband polaritons.

based on total internal reflection. In this work, a transfer-matrix formalism was used to describe the polariton anti-crossing between the cavity optical mode, and the ISBPs formed in a GaAs/AlGaAs quantum well-based structure. Using electrical injection in a quantum cascade LED based also on GaAs, Sapienza *et al.*[44] later demonstrated resonant injection of electrons into the polariton states and used a phenomenological model to explain the results.

The first quantum theory model describing the interaction between the ISBT and a planar microcavity photon mode was reported by Ciuti *et al.*[40] In their seminal work, the concept of ultra-strong light matter coupling was introduced, and the authors identified the relative Rabi energy, i.e., the ratio between the Rabi energy and the matter excitation energy (E_{matter}), as the relevant parameter to access the ultra-strong coupling regime. However, this model did not account for the collective oscillations, i.e., ISBPs, hence overlooking the effect of depolarization. This effect was later accounted for in the work by Todorov *et al.*,[34] who used a quantum model to determine the polariton dispersion relation as well as the coupling strength. The full quantum theory describing the coupling between ISBTs in a two-dimensional electron gas and a photonic cavity mode was later published by Todorov and Sirtori,[33] who accounted for the Coulomb interaction between electrons in different subbands. In this model, they showed that it is the actual phase-locked collective electronic transitions acting as a plasmonic mode that couple to the photonic mode of the cavity.

The first experimental demonstrations of the ultra-strong coupling regime were performed using ISBPs.[34,45,46] It was shown[33,47] that the Rabi energy is proportional to the plasma energy of the electron gas (E_P), as $E_R = \sqrt{f_w}\, E_P$, where $0 \leq f_w \leq 1$ is the spatial overlap between the photonic mode and the matter polarization. The relative Rabi energy is thus given by

$$\frac{E_R}{E_{matter}} = \frac{\sqrt{f_w}\, E_P}{\sqrt{E_{conf}^2 + E_P^2}} \leq 1. \tag{6}$$

Here, E_{conf} stands for the contribution of confinement effects to the excitation energy $\sqrt{E_{conf}^2 + E_P^2}$. Therefore, Eq. (6) holds for intersubband plasmons (with, in this case, $E_{conf} = E_{ISBT}$), multisubband plasmons ($E_{conf} = E_0$) and Berreman modes ($E_{conf} = 0$). It clearly shows the interest of increasingly collective effects, thus the plasma energy, with respect to single particle transition energies. Indeed, the introduction of MSPs allowed reaching unprecedented values of the relative Rabi energy,[11,12,17] even though the existence of an upper limit for the relative Rabi energy for MSPs prevents the system from reaching the deep strong coupling regime,[48] that requires $\frac{E_R}{E_{matter}} \geq 1$.

The ultra-strong coupling between the MSP, at energy E_{MSP}, and the cavity mode, at energy E_c, produces two polariton modes given by the following expression:[11]

$$E_{UP/LP}^2 = \frac{1}{2}\left(E_c^2 + E_{MSP}^2 \pm \sqrt{(E_c^2 - E_{MSP}^2)^2 + 4E_R^2 E_c^2}\right). \tag{7}$$

Figure 4(b) shows the polariton branches for a relative Rabi energy $E_R/E_{MSP} = 0.5$. The two branches are separated by a photonic reststrahlen band where no modes can exist, defined between the lower limit given by $\sqrt{E_{conf}^2 + E_P^2(1 - f_w)}$, and the higher limit given by E_{MSP}. This energy gap can be explained as the result of the destructive interference between the microcavity electromagnetic field and the MSPs.[33] When the $E_{MSP} = E_c$ condition is met, both polariton branches are equally photonic and plasmonic in character, and the maximum plasmon–photon intermixing is obtained. As the cavity energy is decreased, the upper polariton branch retains a highly plasmonic character, whereas the lower polariton branch remains mostly photonic. In contrast, for large cavity energies, the upper polariton branch becomes highly photonic in nature, whereas the lower one becomes highly plasmonic.

Recalling the dependence of the effective plasma frequency of the MSP on the two-dimensional electron concentration [Eq. 3(a)], we notice that the Rabi energy scales as $\sqrt{\Delta n_{2D} f_w}$, i.e., a high coupling strength is obtained for large electron concentrations. This result is equivalent to that of the MSP polaron from the previous Section, but, in contrast to that case, the coupling in the MSP polariton also depends on the spatial overlap between the photonic mode and the matter polarization, f_w. Assuming an optical mode that fills homogeneously the entire cavity, f_w would be given by the ratio of the volume of the material where the MSP exists ($n_{QW}L_{QW}$) to the cavity thickness (L_{cav}), i.e., $f_w = n_{QW}L_{QW}/L_{cav}$. The desire to have a photonic mode that fills entirely the optical cavity sets a requirement on the type of cavity that can be used. If the cavity is defined vertically, like in the work reported in Refs. 43 and 44, the cavity vertical length has to be at least of the order of half the light wavelength divided by the index of refraction of the material. This implies that for MSPs in the mid-IR, optical cavities one to several micrometers thick are required, a thickness that needs to be dramatically increased toward the THz. Hence, a very large number of quantum wells have to be used, which can be a technological issue for certain material platforms (see Sec. V). This problem can be circumvented by enclosing the multiple quantum well structure between a bottom metal layer and metal stripes[47] or 0D micro-patches,[11,12,34] with vertical dimensions much smaller than the electromagnetic wavelength, yielding a microcavity polariton. Under these configurations, the electromagnetic field intensity would be constant along the cavity [like that shown in Figs. 4(a) and 4(c)], and the cavity length would be entirely filled by a TM mode. Indeed, with this type of cavity, the ultrastrong coupling regime can be reached, with values for the Rabi energy normalized by the MSP energy as large as $\frac{E_R}{E_{MSP}} \approx 0.41$ for a multiple quantum well structure containing six confined energy levels,[11] or even ≈0.73 when using a structure with a Berreman mode.[12]

As mentioned above, the signature of the ultra-strong coupling regime is the appearance of the photonic gap. This property can be used to create materials with an artificial reststrahlen band.[12] In the ultimate limit of the ultra-strong coupling regime ($\frac{E_R}{E_{MSP}} = 1$), the energy of the lower polariton branch vanishes, and the forbidden band spans from 0 to the plasma edge E_P, which corresponds to the metallic limit.

The ultra-strong coupling also pushes down the lower polariton branch at energies degenerate with the optical phonon modes [see Fig. 4(b)]. This resonance gives rises to a new strong interaction which mixes electrons, phonons and photons, giving rise to

new collective modes. The original reststrahlen band of the material is, therefore, modified by the strong interactions that renormalize the phonon energies. For sufficiently high values of the relative Rabi energy [Fig. 4(b)], the lower polariton states possess a non-negligible matter fraction in the THz region. The ultra-strong coupling thus provides a way of transferring oscillator strength from the mid-infrared region, where the resonances of MSPs takes place, toward the far infrared.[17] This approach opens the way toward the realization of efficient THz devices with an enhanced light–matter interaction by exploiting the ultra-strong coupling regime.

An important perspective for microcavity polaritons based on MSPs is the possibility of realizing polariton lasers[49,50] in the THz domain. Indeed, owing to their bosonic character, these quasi-particles undergo stimulated scattering toward a final state. For exciton–polaritons, one of the mechanisms that have been exploited for stimulated scattering is optical phonon assisted relaxation into a minimum of the polaritonic dispersion curve.[51] It was theoretically shown that optical phonons can be also at the origin of stimulated scattering of intersubband polaritons.[52] This scheme is at the basis of recent proposal for midinfrared lasers without electronic population inversion.[53] Two different approaches have been investigated. The first employs electrical pumping to excite the upper polariton branch, from where polaritons relax through phonon scattering and populate the lower branch.[54] This approach takes advantage of quantum engineering techniques typical of unipolar devices to design the electronic injector. The second approach relies on optical pumping in carefully designed optical cavities that present a minimum in the dispersion.[55] Note that neither approach has shown up to now experimental evidence of stimulated coherent emission. More recently, scattering between intersubband polaritons in a dispersive cavity has also been experimentally evidenced,[56] and identified as a possible mechanism leading to bosonic lasing. An alternative way to go farther is to combine MSPs with 0D metamaterials in order to break optical dispersion and provide at resonance two polariton states separated of an optical phonon energy, as sketched in Fig. 4(d).

V. MATERIAL PLATFORMS

In Secs. II–IV, we have shown that MSPs and their applications lie at the interface between different scientific fields, from nanoplasmonics to semiconductor physics. In this section, we explore the different material properties required to define the ideal material platform, which would simultaneously address these topics. We discuss the trade-offs to achieve this goal. And, by turn, we will be able to define a specific "maturity level" to identify the future material platforms. As a guideline, we can view this optoelectronic domain as sharing some features with unipolar devices such as: (1) the control of the quantum heterostructures and the conduction band offsets; (2) the control of the electron densities; (3) an advanced technological know-how for the device processing. But it may differ from quantum cascade devices in terms of transport, influence of interface disorder, or quantum well doping such that the best materials for MSPs are not necessarily the same as for quantum cascade devices.

A. Figures of merit: Intrinsic properties and doping

By considering the plasma energy E_p given in Sec. II [Eq. (3a)], the strength of the transition relies on three main parameters: ε_∞ the high frequency dielectric constant, m^* the effective mass of the material, and n the electron density. ε_∞ and m^* are intrinsic properties of the considered material. In turn, n can be in some cases related to the technological maturity of the growth processes—i.e., higher n could be achievable, we just do not know yet how to reach it—whereas, for some other materials, it looks like the absolute maximum of n has already been reached—e.g., GaAs, a very technologically mature material for which $n \sim 10^{19}$ cm^{-3} is hardly achievable. Therefore, two distinct figures of merit can be defined: (1) FOM_i depending only on the intrinsic properties ε_∞ and m^*, and (2) FOM_n for which the maximum electron density is considered,

$$\text{Intrinsic}: FOM_i = \sqrt{\frac{1}{\varepsilon_\infty m^*}}, \tag{8a}$$

$$\text{With } n: FOM_n = \sqrt{\frac{n}{\varepsilon_\infty m^*}}. \tag{8b}$$

For sake of clarity, the figures of merit are normalized to that of GaAs in the following discussion. The ideal materials would be those with both ε_∞ and m^* as low as possible. A classification of materials can be established as a function of the bandgap E_G as shown in Fig. 5. FOM_i (full black circles in Fig. 5) exhibits a weak dependence with E_G because ε_∞ and m^* vary in an opposite way as a function of E_G in semiconductors. Only materials with very large dielectric constant and/or effective mass will show a different behavior of FOM_i (e.g., as oxide perovskites for instance). A very important parameter is then the ability to control the electron density at a very high level ($n > 10^{19}$ cm^{-3}) as evidenced by FOM_n (open red squares in Fig. 5). This strong condition is a prerequisite to define the ideal material for MSPs. Two classes of materials emerge here: (1) III-As semiconductors with InAs quantum wells

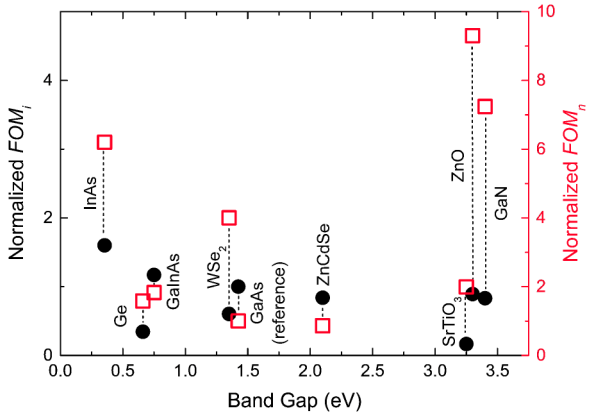

FIG. 5. Figures of merit of different material systems as a function of the bandgap, normalized to that of GaAs. Full black circles: intrinsic FOM_i given by (8a); Open red squares: FOM_n given by (8b).

thanks to their low m^*, and (2) wide bandgap semiconductors (nitrides and oxides) due their low ε_∞ and the ability to be highly doped.

Achieving high carrier density is not straightforward and requires a thorough optimization of the growth process for the dopant incorporation. By increasing the dopant concentration, extended defects can be nucleated and can degrade the optical and transport properties. A large difference between the dopant concentration and the carrier concentration is also often observed due to strong compensation mechanisms in all materials.[57,58] Sometimes, the compensation can be overcome or strongly limited by changing the growth method. For instance, Brochen *et al.* have shown that the use of molecular beam epitaxy instead of metal organic chemical vapor deposition could reduce the compensation level in ZnO and limit it at a low level even at a very high donor concentration.[59] The dopant itself can be chosen to limit the compensation. In (Al,Ga)N alloys, several groups have reported an increase of the carrier concentration in the alloy by almost one order of magnitude by changing the donor from Si to Ge[60] and, by turn, limiting the compensation of vacancies complexes.[61] In wide bandgap semiconductors, the ionization energy of the dopants is often an issue. While in III-As the ionization energy of Si in GaAs is about a few meV, it reaches 12 meV in GaN[62] and 25 meV in $Al_{0.85}Ga_{0.15}N$.[63] Nevertheless, for MSPs, the minimum required carrier concentration is above the Mott transition of the considered materials. Therefore, the activation energy of dopant vanishes in this case. Altogether, it is not straightforward to give a precise value of the maximum reachable carrier concentration for each material system, but the estimation used for the calculation of the *FOM* is given in Table I.

B. Technological bandgap engineering: Materials for heterostructures

In addition to the bulk properties of the active materials, the MSP regime obviously requires the ability to manage heterostructures and bandgap engineering. Although quantum well heterostructures have been demonstrated in many material systems, evidence of intersubband transitions is available in a much smaller number of materials, which for the case of MSPs is even lower. Each material system experiences specific limitations, but most of them can be summarized as: (1) issues to obtain a barrier (alloy) and interfaces; (2) strain and relaxation. Moreover, the barrier height (conduction band offset) plays a major role in the design of MSP-supporting QWs. MSPs are realized based on high electron density in a QW, and the typical Fermi level for mid-infrared MSPs is of order of a few hundreds of meV above the conduction band minimum. Potential future realizations in the near infrared are even more demanding since the carrier concentration should be at the upper limit of every material system. We next will focus on the material systems discussed above, addressing the current status and the novel opportunities.

1. III-V compounds

Indium-based III-V material systems—namely, InAs/AlSb and GaInAs/AlInAs lattice-matched to InP—are particularly well suited for the implementation of MSPs. They benefit from a high technological maturity and have been extensively used for the realization of quantum cascade lasers. They can be electron-doped at high densities, and already constitute a platform of choice for the realization of dense two-dimensional electron gases (2-DEGs). Indeed, collective effects between two subbands were originally observed in an InAs/AlSb QW,[64] and the first implementation of MSPs was realized in a GaInAs/AlInAs QW.[11] The GaInAs/AlInAs platform has been used for the most advanced demonstrations based on MSPs, from electrical injection to superradiant emission, as described in other sections of this paper. On the other hand, the InAs platform exhibits very promising advantages, first in terms of technologically controlled electron density ($n \sim 10^{20}$ cm^{-3}, which should enable $E_P \sim 1$ eV), and second in terms of barrier height (about 1.8 eV). Therefore, we envision this material system to be the first one to allow demonstration of MSPs at shorter wavelengths. Finally, the GaAs/AlGaAs benefits from a comparable technological maturity, although with smaller achievable electron densities to date ($n < 10^{19}$ cm^{-3}) and a limited barrier height of ~400 meV.

2. Wurtzite nitride semiconductors

As shown in Fig. 5, wurtzite GaN and ZnO are intrinsically appealing for MSP applications. Both share the same crystal structure. For GaN, the barrier is AlN and its related alloy (Al,Ga)N. The barrier height in GaN/AlN is as high as 1.72 eV. Driven by the scientific demonstration of blue LEDs[65] and commercial success of white LEDs, the growth processes have known a rapid development, and both ISBTs and quantum cascade devices based on GaN/(Al,Ga)N/AlN heterostructures have been demonstrated.[66] Recently *n*-type GaN has been obtained with Ge, to limit the compensation experienced with Si dopants, and ISBTs have been observed.[67,68] This material system may be limited for MSP use because of the lack of inexpensive substrates. Usually, these structures are grown on sapphire or Si, giving rise to very large dislocation densities. Recently, Monavarian *et al.* have demonstrated that ISBT absorption energies and linewidth were impressively robust in regards of the structural quality.[69] Yet, no device and no transport have been demonstrated with defective samples. Another limitation of the GaN/(Al,Ga)N heterostructure could be the strain generated by the lattice mismatch between GaN and (Al,Ga)N barrier (up to 2.5% for AlN). Recently, a lattice matched alloy $Sc_{0.18}Al_{0.82}N$ on GaN with even higher barrier height than $Ga_{0.18}Al_{0.82}N$ has been reported using MBE and MOCVD.[70–72] Due to the ferroelectric properties of the barriers, studies are mainly limited to transport of 2-DEG but it offers new perspectives for GaN-based ISBT devices, including the MSP field. Finally, nitride wide bandgap semiconductors benefit from a well-established device processing technology. Despite all the advantages of the nitride material system, no MSP regime has been observed yet.

3. Wurtzite oxide semiconductors

For wurtzite ZnO-based heterostructures, the barrier is (Zn, Mg)O. Here, ZnO differs from GaN. Indeed, the incorporation of high Mg concentration leads to a phase transition because MgO is cubic. Therefore, the Mg concentration is usually limited to $x_{Mg} = 0.5$, giving rise to a ~4.5 eV bandgap. A way to increase the critical concentration has been theoretically suggested by the

TABLE I. Parameters used in Sec. V. PVSK denotes perovskites.

		III-V			II-VI			III-Nitrides		IV	2D	PVSK
		$Ga_{0.47}In_{0.53}As$/InP	InAs/AlSb	GaAs	ZnO	ZnCdSe/InP	Cubic ZnO	GaN/AlGaN	Cubic GaN	Ge/SiGe	WSe_2	$SrTiO_3$
Material constants	ε_∞	11.6	11.7	10.8	3.6	7.3		5		15.8	4.2	5.2
	m^*	0.043	0.023	0.064	0.24	0.134		0.2		0.37	0.45	4.8
Doping	Max doping level ($\times 10^{19}$ cm^{-3})	1.6	10	0.7	72	0.7	?	50	?	14	30	100
	Corresponding Fermi energy (eV)	0.5	3.4	0.2	1.2	0.1	…	1.1	…	0.3	0.4	0.1
	FOMn (a.u. relative to GaAs)	1.8	6.2	1.0	9.3	0.9	…	7.2	…	1.6	4.1	2.0
	Maximum E_P (eV)	0.3	1.1	0.2	1.6	0.1		1.3		0.3	0.7	0.4
Heterostructures	Barrier material	AlInAs (48% Al)	AlSb	AlGaAs (45% Al)	ZnMgO (45% Mg)	ZnCdMgSe (also ZnSe)	MgO	AlN, AlGaN, AlScN	AlN, AlGaN, AlScN	SiGe	Any (in particular hBN)	$LaTiO_3$
	Barrier height (CB offset) (eV)	0.52	1.8	0.39	0.6	≤ 1.2	≤ 3.6	1.75 (AlN)		~0.15	Several eV	2.4
	Quantum cascade structures	Yes	Yes	Yes	Yes	Yes	No	Yes	No	Yes	No	No
	MSP observed in absorption?	Yes	Yes	Yes	Yes	No	No	No	No	No	No, but interband polarons	ISB
	MSP observed in emission? (horizontal transport)	Yes	…	Yes	No	No	No	No	No	No	No	No
	Other important demonstrations	Superradiance	…	…	…	…	…	…		…	…	…
Phonons	LO Phonon energy (meV)	34	30	36	72	31		92		No	30	
	Reststrahlen (meV)	5	2.4	2.2	22.6	6.2		22.9		0	0	
	MSP-polaron	Yes										

fabrication of a BeMgZnO quaternary alloy for which a conduction band offset of almost 2 eV can be achieved.[73] An advantage for ZnO is that the strain is limited when the (Zn,Mg)O/ZnO heterostructure is grown along the *c* axis (the polar direction), since the in-plane parameter depends weakly on the Mg concentration.[74] For MSP applications, ZnO can be highly doped and plasmonics at telecom wavelength has been demonstrated.[75] In addition, (Zn,Mg)O/ZnO heterostructures for NIR and THz have been developed by MBE and ISBTs has been observed.[76–78] Recently B. Hinkov *et al.* have reported a full device processing of ZnO quantum devices,[79] and both a quantum cascade detector[80] as well as emitters[81] have been demonstrated. Since MSPs have already been demonstrated[21] in ZnO, this material platform may be the next one to demonstrate MSP-based devices.

4. Internal electric field and cubic wide bandgap semiconductors

Due to their crystal structure and the strain generated in wurtzite heterostructures, QWs may evidence the presence of a strong built-in electric field when grown along the *c* axis. The origin is associated to piezoelectricity and spontaneous polarization.[82,83] In a heterostructure, it strongly affects the optical properties[84,85] and, by turn, non- and semi-polar wide bandgap semiconductors have been suggested for GaN and ZnO.[86] For ISBTs, the internal electric field also leads to a tilted conduction band profile, limiting the oscillator strength and hindering the ability to tune the energy differences between subbands via varying the well width due to the bounded energy of the lowest states.[84] In addition to non- and semi-polar orientations, other solutions have been very recently proposed, such as cubic GaN and ZnO. In particular, ISBTs have been observed in GaN but the crystal quality is still low. Although cubic (Zn,Mg)O/MgO heterostructures have been recently demonstrated,[87,88] no ISBTs have been reported in QWs. It may be of particular interest due to the very large potential barrier height (3.6 eV), still large doping, and cheap available substrates (MgO).[89] All these strategies aim at avoiding the internal electric field. But in the MSP regime, the carrier concentration is so high that the internal electric field might be screened by free carriers.

As an example, Fig. 6(a) displays the conduction band structure of a (Zn,Mg)O/ZnO highly doped quantum well ($n \sim 2 \times 10^{20}$ cm^{-3}) with and without the internal electric field. The effect of the internal electric field on the position of the MSP absorption line and the intensity is shown in Fig. 6(b). For a carrier concentration above $n \sim 10^{19}$ cm^{-3}, both the energy shift and the difference of the absorption coefficients become negligible. As a consequence, the internal electric fields in wide bandgap semiconductors may not be a major issue for unipolar devices, contrary to what is observed in band-to-band optoelectronic devices.

5. IV–IV compounds

Group IV materials have recently attracted interest in efficient ISBT-based light emitters due to the potential integration on Si wafers and the fact that the radiative decay rate does not depend on electron hole recombination in such devices.[90,91] Thanks to the

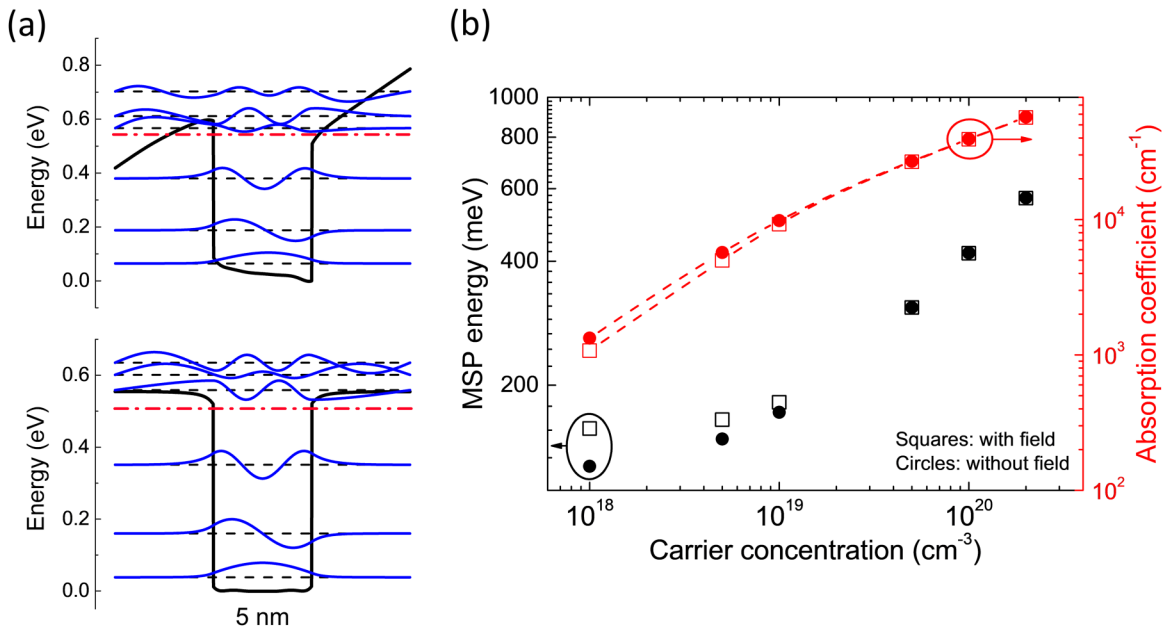

FIG. 6. (a) Conduction band structure of a (Zn,Mg)O/ZnO quantum well with a 500 kV/cm internal electric field (top) or without electric field (bottom). The electron concentration is set to $n \sim 2 \times 10^{20}$ cm^{-3}. (b) Effect of the internal electric field on the MSP as a function of the electron concentration (transition energy and absorption coefficient).

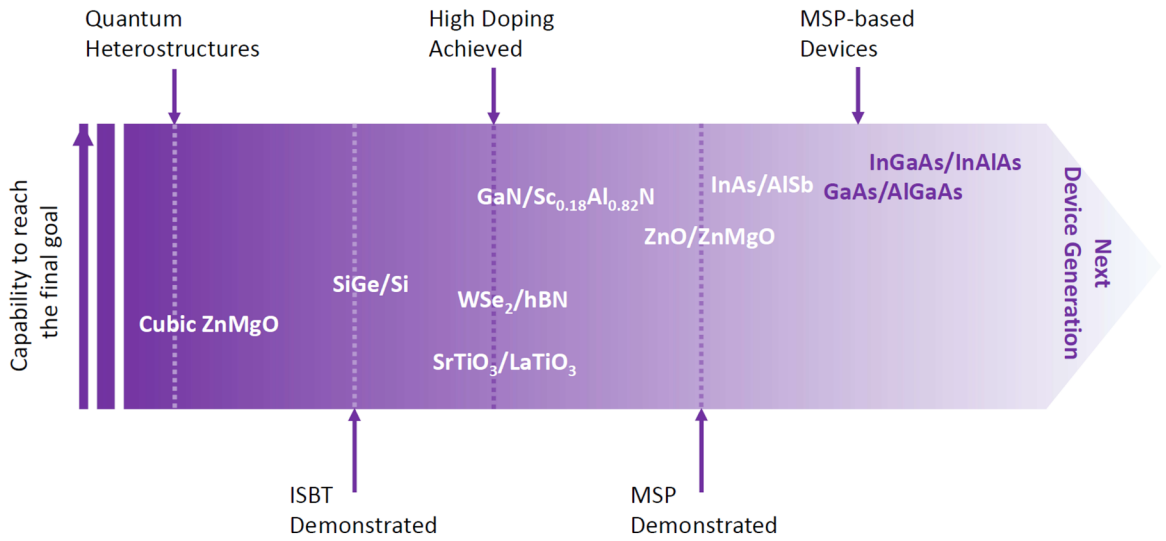

FIG. 7. "Maturity level map" for MSP devices. The lateral scale gives the current status of the material system as a function of the defined milestones.

absence of polar longitudinal optical phonons, SiGe-based ISBT devices are expected to lase at room temperature in the III-V compound reststrahlen band (~ 25–40 meV).[92] Clearly, this material platform is the most mature among all the materials addressed in this article, and electroluminescence in the THz range has been demonstrated.[93] But many challenges still remain, such as the control of the diffusion of *n*-type dopants or the structural quality in strain compensated Ge-rich heterostructures due to the large lattice mismatch with Si substrates.[94] In addition to these challenges, this material system suffers from a limited barrier height and a large ε_∞, which is only partially compensated by a large doping level achievable[95] of $n \sim 1.4 \times 10^{20}\,\mathrm{cm}^{-3}$.

6. Perovskites

Recently, ISBTs have been observed in high quality perovskite heterostructures such as $SrTiO_3/LaAlO_3$ grown by molecular beam epitaxy by Ortmann *et al.*[96] Unfortunately, the FOM_i of such material systems is small ($FOM_i = 0.2$) due to a rather large dielectric constant ($\varepsilon_\infty > 5$)[97] and a huge effective mass ($m^* = 4.8m_0$).[98] But QWs can be highly doped (up to $n = 10^{21}\,\mathrm{cm}^{-3}$) in such material systems,[99] giving rise to $FOM_n = 2$, much better than that of GaAs. Very recently, novel alloys have been suggested for ISBT structures, such as $BaSnO_3$ with lower effective mass and dielectric constant.[100] These material systems may pave the path toward new directions in this optoelectronic field due to their unique multifunctional properties such as ferroelectricity. As a clue of this assertion, $SrTiO_3/LaAlO_3$-based hyperbolic metamaterial structures have already been reported with high FOM in the mid-IR.[97]

7. 2D materials

Two-dimensional (2D) van der Waals materials offer unique possibilities for the realization of heterostructures designed at the level of a monolayer, without the constraints associated with crystal lattice matching.[101] Prominent examples include graphene, transition metal dichalcogenides (TMDs), and black phosphorus. These materials possess appealing optical properties such as strong light absorption, tunable bandgap, and high mobility, making them attractive for optoelectronic applications. The wide-gap insulating material hexagonal boron nitride (hBN) is widely used as an encapsulating material to isolate the optically active region from its environment and can also be used as a tunnel barrier.[102] ISBTs have been experimentally observed in WSe_2 and MoS_2 in multilayers ranging from 1 to 6 monolayers.[103] WSe_2 can be electrostatically doped up to $2 \times 10^{13}\,\mathrm{cm}^{-2}$ per monolayer (i.e., about $3 \times 10^{20}\,\mathrm{cm}^{-3}$),[104] yielding $FOM_n \approx 4$. Collective effect in 2-DEGs in gated TMDs is a very active field of research.[105] These recent results suggest that 2D heterostructures based on TMDs would be an exciting direction for future investigations.

VI. SUMMARY

In this section, we have identified different material systems that can be used for MSP devices in the future. To achieve this goal, the material system needs to be mature in terms of growth technology and device processing, with specific requirements like the high electron density. Only the III-As material platform exhibits such a maturity. All other material platforms are at different levels of development. This discussion can be summarized in Fig. 7, in which we define a timeline from the first realization of a quantum heterostructure to final devices. The path toward this final goal can be defined by five milestones. We have classified the materials discussed above as a function of the position in this "maturity level map". In addition, we estimate the difficulty to reach the final goal considering different parameters such as the maturity for device processing in other application fields, or

bottlenecks like doping limitation. Hence, the material platforms that are closer to the front of the arrow are more likely to become the next generation MSP devices. Clearly, wide bandgap semiconductors appear as the next materials in the game.

VI. SUPERRADIANCE AND DEVICES

The very strong interaction that MSPs have with light is intimately related to their collective nature, i.e., they are a symmetric superposition of all the optically active electronic transitions of the system. This property has major consequences on the spontaneous emission lifetime of an excited plasmon state whose lifetime is shortened proportionally to the number of electrons participating in the collective excitation.

Let us consider a highly doped quantum well, with an electronic density per unit surface N_s, displaying a single bright multisubband plasmon mode at energy $\hbar\Omega_{MSP}$. By using the Fermi golden rule, it is possible to demonstrate that the spontaneous emission rate of the plasmon can be expressed as[20,23,106,107]

$$\Gamma(\Omega_{MSP},\ \theta) = \Gamma_0 \frac{\sin^2\theta}{\cos\theta} = \frac{e^2 N_S}{2\, m^*\, c\, \epsilon_0 \sqrt{\epsilon_\infty}} \frac{\sin^2\theta}{\cos\theta}, \tag{9}$$

with θ being the emission angle measured with respect to the normal to the quantum well plane. The dependence of the spontaneous emission rate on $\sin^2\theta$ comes from the fact that the dipole associated with the bright plasmon mode is oriented along the direction normal to the quantum well plane (i.e., along the growth direction). The dependence on $1/\cos\theta$ is due to the divergence of the photonic density of states in the free space that couple to the two-dimensional plasmon. The angular dependence of the radiative rate allows us to vary the interaction between the plasmon and the electromagnetic field by simply changing the angle of light propagation. As it will be discussed later, this allows experimentally investigating different regimes of the light–matter interaction.

The most peculiar characteristic of the spontaneous emission rate is its linear dependence on the electronic density, N_S, typical of superradiance. Superradiance, first introduced by Dicke in 1954,[108] is the coherent enhancement of the spontaneous emission rate of a quantum emitter owing to the presence of other identical emitters within a wavelength distance (Fig. 8). It was observed in several systems:[109] low-pressure optically pumped gases,[110] cold atomic gases,[111] quantum dots,[112] organic emitters,[113] superconducting transmon qubits,[114] and cyclotron resonances.[115] Superradiance occurs when a dense collection of emitters oscillates in phase: our plasmonic excitations are thus ideal for the observation of this phenomenon, as they are essentially a dense collection of dipolar oscillators, all oriented along the same direction (the confinement direction). This is sketched in Fig. 8. There are two important differences between superradiance in atomic systems and in highly doped quantum wells. The first is that atomic emitters are labelled by their position vectors $\vec{r}$ [Fig. 8(a)], while electrons in quantum wells are so by the in-plane momentum, $\vec{k}$ [Fig. 8(b)]. The second is that the atomic dipoles are randomly oriented, whereas the optical polarization of the electrons is oriented only in the direction of the confinement. These two considerations and the high electron density in the quantum well are at the origin of the very strong dipole-dipole coupling between ISBTs, giving rise to the MSP, characterized by a giant dipole along the growth direction [Fig. 8(b)].[33,116]

The experimental signature of the superradiant behaviour of MSPs is the radiative broadening of the plasmon absorption spectra, which increases with the electronic density, as it has been shown in samples with different doping levels.[20] In particular, the

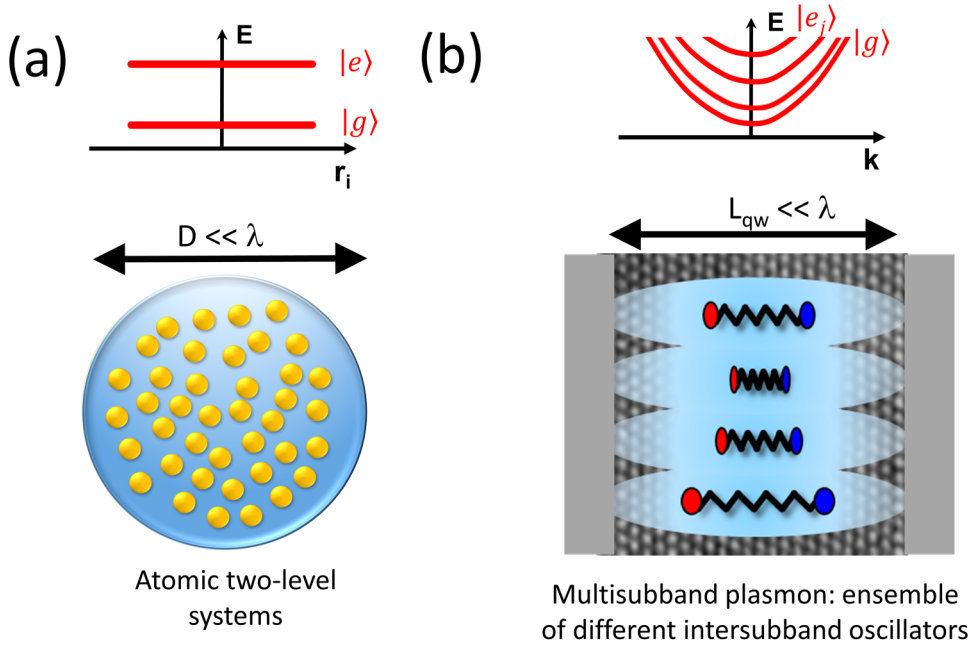

FIG. 8. Comparison between an atomic ensemble and a two-dimensional electronic system. (a) Different atoms are labeled by their position in the real space and have flat dispersion in the momentum space. Superradiant behavior may appear when the atoms are distributed in a distance much smaller than the wavelength. (b) In a quantum well with several occupied subbands, there is also a collection of two-level emitters, which, however, can be recognized by their momentum in the plane, rather than their positions. Coulomb interaction gives rise to a collective mode at energy E_{MSP} displaying a giant dipole along the growth direction.

plasmons can reach a radiative decay time of the order of ∼100 fs. This value is several orders of magnitude shorter than that of the spontaneous emission time of a single electron in the mid-infrared, ∼100 ns. Furthermore, it is much shorter than the characteristic time of any nonradiative scattering event. As a consequence, the energy relaxation dynamics of the plasmon can be dominated by the radiative rate.

As the radiative broadening is larger than the nonradiative one, perturbation theory becomes inappropriate to describe the coupling between plasmons and free-space radiation.[107] The optical properties of the plasmon mode have been calculated by Huppert *et al.*[106] by solving quantum Langevin equations in the input-output formalism. In this model, the bright plasmon is coupled with two bosonic baths: a bath of electronic excitations and a bath of free space photons. The coupling with the electronic bath is considered phenomenologically, and it gives rise to an intrinsic non-radiative broadening γ of the plasmon mode, which is typically 20 times smaller than the plasmon frequency Ω_{MSP}. The coupling between the plasmon and the free space photons is calculated by using a quantum approach, including the antiresonant terms of the light–matter interaction. In the non-perturbative approach, the radiative decay rate also becomes a function of the photon frequency ω,

$$\Gamma(\omega,\ \theta) = \Gamma(\Omega_{MSP},\ \theta)\frac{\omega}{\Omega_{MSP}}. \tag{10}$$

The emission rate $\Gamma(\omega,\ \theta)$ is proportional to that obtained using Fermi's golden rule, provided in (9). In the input–output approach, the radiative decay rate is also frequency-dependent, characteristic of non-Markovian dynamics. Notice that only at resonance, $\omega = \Omega_{MSP}$, the emission rate $\Gamma(\omega,\ \theta)$ coincides with the result obtained by Fermi's golden rule. The interaction between the plasmon and the electromagnetic field can be varied by simply changing the angle of the light-propagation in free space. This allows to experimentally investigate different regimes of the light–matter interaction. Indeed, in analogy with the cavity quantum electrodynamics approach, we can introduce a decay ratio $g = \Gamma(\Omega_{MSP}, \theta)/\gamma$ as a parameter to discriminate among the weak, strong and ultra-strong coupling regime between the plasmon and the free-space radiation. For $g \ll 1$, the plasmon can be considered in a weak coupling regime with free-space radiation. In this case, the non-radiative broadening is dominant with respect to the radiative one, and Fermi's golden rule is suitable to describe the plasmon spontaneous emission. For $g > 0.1$, the perturbative approach becomes less accurate: the system enters the strong coupling regime, while the plasmon linewidth is progressively broadened due to the increase of the radiative decay rate. When not only is $g \gg 1$ but also $\Gamma(\Omega_{MSP}, \theta) \approx \Omega_{MSP}$, plasmons are ultra-strongly coupled with free-space radiation, and antiresonant terms of the interaction are crucial in preventing an unphysical broadening of the plasmon which would reach negative frequencies.

The input–output model allows deriving an analytical formula of the absorptivity. For a single bright plasmon mode, close to a perfect gold mirror, the absorptivity is given by[107]

$$\alpha(\theta,\ \omega) = \frac{\frac{4\ \Omega_P^2}{(\Omega_P+\omega)^2}\ \gamma\Gamma(\theta,\omega)}{(\omega-\Omega_P)^2 + \frac{4\ \Omega_P^2}{(\Omega_P+\omega)^2}\left(\frac{\gamma}{2}+\frac{\Gamma(\theta,\omega)}{2}\right)^2}. \tag{11}$$

This formula can be applied for arbitrary values of the decay ratio g, as illustrated in Fig. 9. This figure presents the results of reflectivity experiments performed on a 150 nm thick highly doped ($2 \times 10^{19}\,\mathrm{cm}^{-3}$) GaInAs layer, on a gold mirror. The red lines in Fig. 9 show the spectra calculated by using (11).[117] Figure 9(b) presents the full width at half the maximum (FWHM) and the maximum absorptivity as a function of the angle, extracted from the spectra. For small angles ($g < 1$), the absorption spectrum has a Lorentzian line shape, whose FWHM is set by the non-radiative broadening. When increasing the angle, the contribution of the radiative broadening on the FWHM increases, and for $g = 1$ the MSP displays perfect absorption: the system is in the critical coupling regime. For angles greater than the critical coupling angle, the plasmon is overdamped: the absorption spectrum is radiatively broadened and the absorptivity peak decreases.

From the previous considerations, it is clear that the existence of a critical coupling regime stems from the superradiant behavior of the MSPs. It is remarkable that this regime can be reached without using any photonic structure, but by only exploiting the coupling of the plasmons with free space radiation. Kirchhoff's law of thermal emission states the equivalence between the emissivity and the absorptivity at a given wavelength and emission angle.[118] As a consequence, MSPs can be used to realize quasi-monochromatic perfect thermal emitters. Thermal emission of MSPs can be induced by Joule heating, by applying a current in the quantum well plane, as depicted in the inset of Fig. 10.[106] In this geometry, heat is generated only in the quantum well layer, through the dissipation of electrical power, and then propagates toward the heat sink at the bottom of the semiconductor substrate maintained at room temperature. A time modulation of the injected current results in the modulation of the incandescent emission. However, due to the low heat capacitance of the electron gas with respect to that of the lattice, the modulation of the electronic temperature through Joule heating can be faster than the heat exchange between the electrons and the lattice. Figure 10 shows the total optical power emitted by a device based on a 45 nm highly doped GaInAs layer, as a function of the frequency at which the injected current is modulated. At small values of the frequency, the heat exchange between the electron gas and the lattice is efficient, resulting in the whole increase of the temperature of the system, and hence of the emitted power. While increasing the frequency, the heat exchange progressively becomes less efficient and, starting from ∼1 MHz, only the electronic temperature is affected by the application of the in-plane current, and the optical power stays constant with the frequency. The thermal emission is modulated up to ∼ 50 MHz, which is only limited by the bandwidth of the detector used for the experiment, as shown in Ref. 117.

The devices for thermal emission presented before are reminiscent of the geometry used in field effect transistors. This

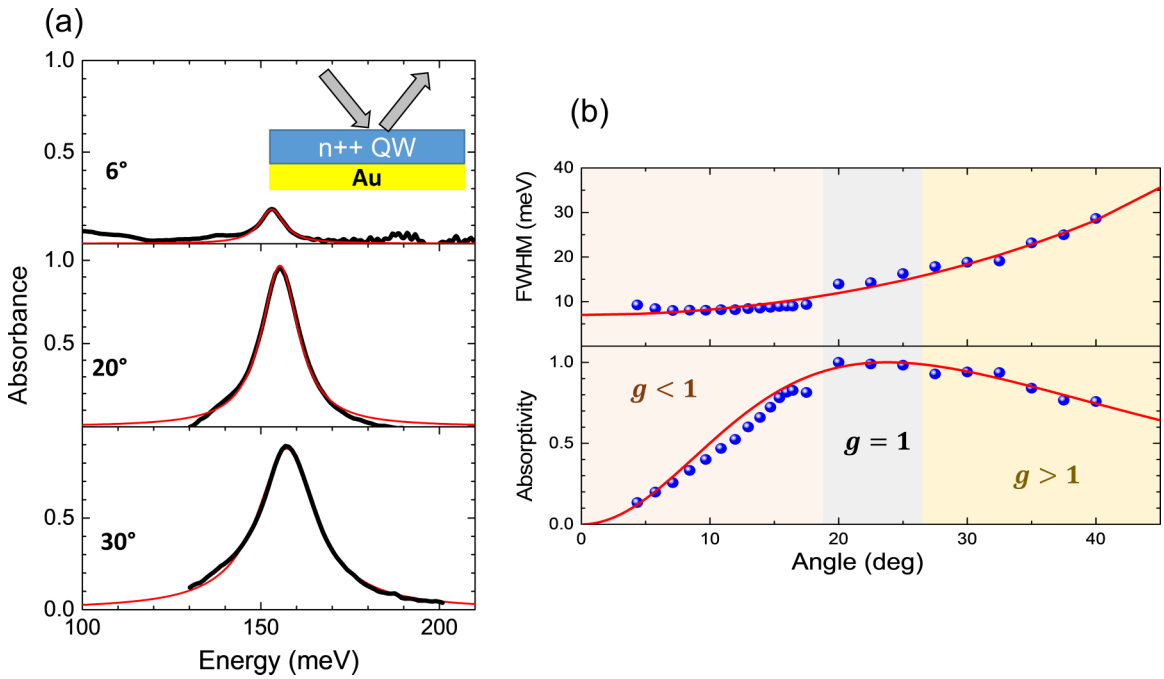

FIG. 9 (a) Absorption spectra, extracted from reflectivity experiments, at three different internal angles (black lines) and Lorentzian fit of the resonances (red lines). The inset presents a sketch of the geometry used for reflectivity experiments. (b) Top panel: full width at half the maximum (FWHM) of the absorption peak (blue symbols) as a function of the internal angle. Red line presents the calculated broadening, including radiative and nonradiative contribution. Bottom panel: peak absorptivity extracted from the absorption spectra as a function of the angle, compared with the calculated one (red line) by using Eq. (11).

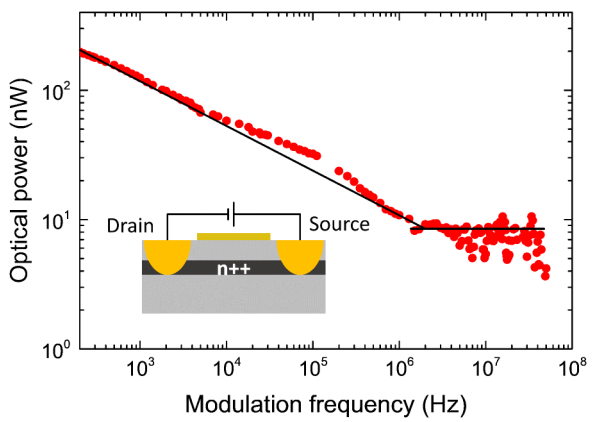

FIG. 10. (a) Emitted power as a function of the modulation frequency (dots). The solid line is a guide for the eye highlighting the existence of two different regimes in the device operation. At low frequencies, the application of an in-plane current induces an increase of both the electronic temperature and the lattice one. For frequencies above ~1 MHz, the current modulation only induces an increase of the electronic temperature, and the emitted power becomes independent on the modulation frequency. The inset presents a sketch of the device.

similarity raises the question if superradiant thermal emission could be also induced in Si devices based on CMOS technology, to enable their radiative cooling. This would have immense repercussions in dense electronic systems which are fundamentally limited by the temperature increase due to internal thermal dissipation. As a matter of fact, transistors present channels with electron or hole densities in the order of 10^{13} cm^{-2} and several confined energy levels are occupied. The associated MSPs can emit in the THz range between 5 and 30 THz. A THz emission in a Si MOSFET induced by thermal effects[119] has already been observed in the 70s, even though the emission was not associated to superradiance. However, this collective effect is the essential ingredient to provide an efficient thermal emission, thus cooling.

The emission described until now is of thermal nature and it is based on Kirchhoff's law. It is therefore an incandescent emission imposed by the difference between the temperature of the electron gas and that of the lattice and by the emissivity of the system. Incandescent emission is limited by blackbody efficiency set by Planck's law. A cold emitter would be an ideal solution to go beyond this limitation. This implies that plasmons should be excited with a resonant transfer of energy that brings them into the excited state from where they radiatively relax. A dc electrical current would be the ideal source of resonant excitation: in this regime photons are emitted every time electrons transfer their

kinetic energy to the plasmon. This sets a linear dependence of the emitted power on the current, which can be considered as the experimental signature of resonant injection.[120] Moreover, the direct excitation of the plasmon does not imply a change in temperature and will not be limited by blackbody emission. This non-thermal light generation would fully exploit the superradiant character of the plasmon and give birth to the first cold emitter in the THz range. However, the engineering of a cold source based on superradiant MSPs is a challenging problem. Several theoretical questions are still open: What mechanism ensures the energy transfer from electrons to plasmons? Is it possible to exploit resonant tunneling to design an efficient injector, as it is the case for several unipolar quantum devices, like quantum cascade lasers?

A strategy to experimentally address the fundamental question of the coupling between a fermionic current and a bosonic excitation could be the investigation of quantum cascade detectors based on MSPs. In these devices, plasmons are optically excited, and the current induced by photogenerated electrons, issued from plasmon relaxation, is measured. Electronic transport is ensured by an extraction region, consisting of several electronic levels in tunnel coupled quantum wells. The study of the detector responsivity as a function of the energy position of the extractor levels could provide hints on the design strategies to realize optoelectronic MSP devices. Preliminary studies in this sense have already been performed with intersubband plasmons strongly coupled with a microcavity mode.[121,122] More recently, the first device based on a Berreman mode that can be operated both as an electroluminescent device and as a photodetector has been demonstrated.[123] The device consists of a 100 nm highly doped GaInAs layer, embedded between AlInAs barriers. The sample is processed into a mesa device for the application of a bias along the growth direction. Figure 11(a) shows the absorption spectrum of the sample, calculated for $\theta = 30°$, which corresponds to the critical coupling angle. Figures 11(b) and 11(c) present the photocurrent spectrum and the electroluminescence spectrum, respectively, measured at 7 K.[123] These spectra present the same resonance and the same shape as the absorption spectrum, thus demonstrating that the realization of optoelectronic devices based on Berreman modes, or more generally on MSPs, is possible. Further investigation is needed to optimize the design of such devices in order to increase their efficiency.

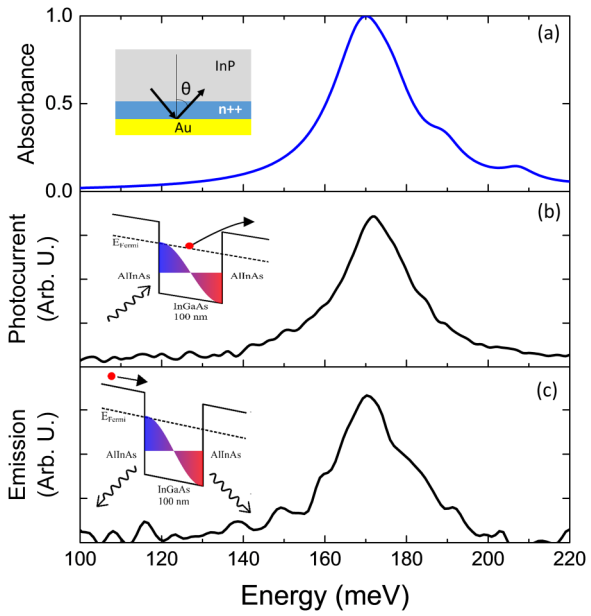

FIG. 11. (a) Simulated absorbance of a GaInAs 100 nm layer, with an electronic density of 2×10^{19} cm^{-3}. The simulation is performed for $\theta = 30°$ and in the presence of a gold mirror. (b) Photocurrent spectrum measured at 7 K. Light from a blackbody source is injected through a 30° facet. (c) Emission spectrum measured at 7 K and 30° internal angle under the application of a bias along the growth direction.

VII. QUANTUM PLASMONIC METAMATERIALS

One of the areas where MSPs will likely excel is in quantum plasmonics and metamaterials, where MSPs show additional desirable features compared to traditional plasmonic structures, such as those based on metals. The key aspect in this case, as we have discussed throughout this perspectives article, is the additional degree of freedom characteristic of MSPs, quantum confinement,[14,22] which allows controlling the behavior of the structure or device. The quantum confinement arises from decreasing the size of the plasmonic system, hence confining the plasmon within an electrostatic potential. The quantum confinement is responsible for the E_0 term in Eq. (4), and as we discussed earlier, can be tuned through either the thickness of the quantum well layer, or the height of the confinement potential. This confinement potential may be controlled by varying the bandgap energy of the barrier layers via different alloy compositions, or by sandwiching the quantum well between undoped layers of the same semiconductor.[117]

In order to illustrate the quantum control of the observable plasmonic transition, let us take as an example the case of a material platform that allows very high electron densities, and hence very high plasma frequencies, the ZnO/$Zn_{1-x}Mg_xO$ system. In this system, the conduction band confinement potential can be as large as 0.51 eV when the barrier is the ternary $Zn_{0.7}Mg_{0.3}O$,[21] which we will use here for the calculations.

For a 50 nm-thick quantum well doped with 3×10^{19} cm^{-3} (well below the maximum achievable doping in this material platform, see Sec. V), quantum confinement and energy level spacing in the QW are very small [Fig. 12(a)], and the MSP resonance is observed at 215 meV, very close to the plasma energy. However, when we increase the weight of the quantum confinement contribution by reducing the quantum well thickness down to 4 nm, while keeping the same three-dimensional electron density in the quantum well, the MSP is excited at an energy of 270 meV. Hence, just by reducing the system size, the plasmonic resonance can be tuned by an additional 55 meV, i.e., by roughly 25% of the plasma energy. The interplay between quantum confinement and electron concentration is evident from Eqs. (3b) and (4), which serve as tool to control the energy of the MSP. When lower electron concentrations are used, quantum confinement provides larger tunability of the final MSP transition energy.

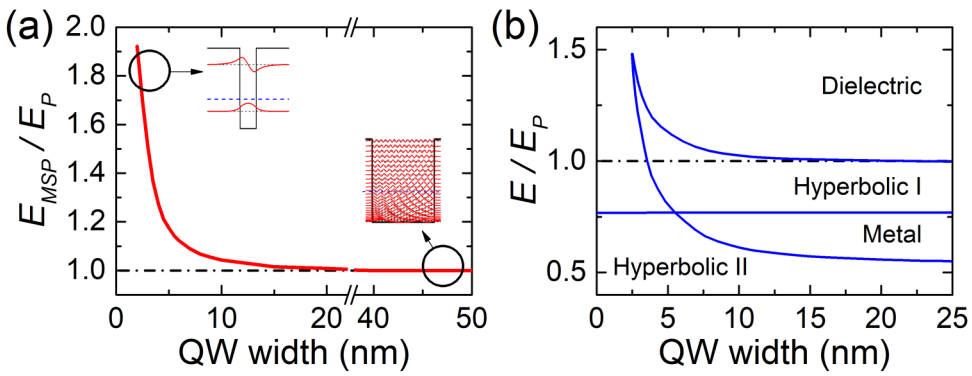

FIG. 12. (a) Dependence of MSP on quantum confinement, calculated with the MSP model. The values of E_{MSP} are normalized to the plasma energy. (b) Optical phase diagram of a metamaterial whose optical response is controlled by the quantum confinement of the MSP. The blue lines represent the frontiers between the different optical phases. The energy values are normalized to the plasma energy.

This degree of quantum control over the observed plasmonic resonance provided by the MSP clearly opens the door for building new metamaterials with unexpected behaviors. By vertically stacking quantum wells, a metamaterial can be built whose in-plane and out-of-plane components of the dielectric function can independently be tuned: the in-plane component via electron concentration, and the out-of-plane component via both electron concentration and quantum confinement.[22] Indeed, using the effective medium approximation[124] these components can be expressed as

$$\varepsilon_{in\ plane}^{effective} = \left(\frac{1}{t_{barrier}+t_{QW}}\right)\left(t_{barrier}\varepsilon_{barrier}+t_{QW}\varepsilon_{in\ plane}^{QW}\right), \quad (12a)$$

$$\frac{1}{\varepsilon_{out\ of\ plane}^{effective}} = \left(\frac{t_{barrier}}{\varepsilon_{barrier}}+\frac{t_{QW}}{\varepsilon_{out\ of\ plane}^{QW}}\right)\left(\frac{1}{t_{barrier}+t_{QW}}\right). \quad (12b)$$

To arrive at these equations, the dielectric function of the barrier is considered isotropic and independent of the energy, whereas that of the QW is anisotropic and has in-plane and out-of-plane components given by Eqs. (1a) and (1b). With a proper choice of the QW/barrier thickness, electron concentration in the QW, and barrier height, the sign of the dielectric function components can be chosen independently, and the metamaterial can therefore be designed to behave as a metal, dielectric, or as a type I or type II hyperbolic metamaterial. In these systems, the control of the quantum confinement via QW thickness and barrier height allows to tune the MSP energy through the confinement contribution (E_0) allowing the control of the optical phase diagram of the system [Fig. 12(b)].[22] This concept may be extended to the different material platforms discussed earlier, hence providing a means to build structures with all types of optical responses, but directly integrated within the devices. Hence, one can envision different structures and devices, with a monolithically integrated metamaterial based on MSPs, which allows to control the properties of light, including polarization state, intensity, or wavefront shape, not only by a priori design of the structure, but also through external control of the MSPs.

The feature that makes MSPs unique for plasmonic applications—namely, the possibility to control the energy of the resonance via the quantum confinement in the QW—has also other peculiarities than can be employed to generate metamaterials and devices with added functionalities. Considering that the MSPs consist of dipoles oscillating along the axis perpendicular to the QW, therefore they only respond to oscillating electric fields in that direction. This selection rule regarding the polarization of the light with respect to the QW plane adds an extra geometrical ingredient for the development of metamaterials.

Take, for example, the work by Montes Bajo *et al.*[125] where a non-planar metamaterial is used to demonstrate a light polarization-sensitive mid-infrared metamaterial operating at normal incidence. In this work, ZnO/ZnMgO QWs are grown on a native m-plane substrate, a configuration in which QWs grow spontaneously with a zig-zagged, grooved-shape oriented along the c axis, which lies in-plane. This feature gives an extra degree of tunability to the MSP structures mentioned up to now, because on top of providing control of the optical phase of the metamaterial, these structures absorb light at normal incidence, but only if the light is polarized perpendicular to the c axis, adding a degree of sensitivity to polarization at normal incidence that otherwise will not be possible.

The previous example illustrates how a detailed design of the geometry of the structure, beyond stacking layers of different materials, or accompanied by technological processing, opens a path to design devices in a way that was not considered in full before. Indeed, as the properties of MSPs depend on those of their constituting electrons, one can tailor the optical spectrum through the electronic potential. For example, designer metamaterials based on MSPs could be created by exploiting tunnel coupled quantum wells. In this way, the techniques typical of band-structure engineering can be transferred to the realm of quantum plasmonics to create active devices. Furthermore, all the micro- and

nano-fabrication techniques currently used for semiconductor devices can be employed to fabricate antennas and photonic structures.[126] All this, together with the quantum plasmonic characteristics of MSPs, will make them a very attractive physical platform for the metamaterials research community in the mid-term.

As mentioned above, another aspect that makes MSPs appealing in metamaterials and quantum plasmonic structures will be the possibility to control the behavior of the structures, in terms of resonance frequency, optical phase or by switching the device on or off by an external means, such as temperature, electrical bias or optically. From an engineering point of view, this looks like the route to be explored since it will shift the topic from solid state physics or light-matter-interaction to the realm of applied physics and devices. Some ideas in this regard are being attempted by the community, as overviewed below.

Man *et al.*[127] have reported a polaritonic metasurface composed of sub-wavelength patch antennas coupled to intersubband transitions from InGaAs/InAlAs MQWs, to achieve nonlinear saturable absorbers and reverse saturable absorbers[128] in the mid-IR with a response time below 2 ps, dictated by the intersubband dynamics. In their work, and building on previous reports where the degree of coupling strength is controlled by optically changing the electron density in the QW,[9] they optically control the coupling strength between the antenna resonance and the intersubband transition by depleting the ground energy state in the quantum well through light absorption. At a low incident light intensity, the strongly coupled nanoantenna-ISBT system yields two split polariton branches (see Sec. IV), and the incident light is fully reflected, whereas at high light intensities, the ISBT is saturated and the antenna is no longer strongly coupled to it, yielding strong light absorption at the antenna resonance energy. By using a MSP, this concept could be extended to higher energies or regimes with higher incident light power.

One step further in complexity, but also in flexibility, is to use an electrical bias to control the MSP. The notion here is to control the MSPs by depleting the carrier concentration in the QW levels. To do so, a Schottky contact can be used, whose associated depletion region can be controlled with an electrical bias, and hence, by placing the QWs within the depletion region[129,130] the absorption of the MSP can be modulated. This idea faces the challenge that only the QWs closest to the Schottky contact can be significantly depleted. This concept has been used, though, to modulate the index of refraction in the NIR by controlling with an external bias the ISBT from GaN/AlN QWs.[131] One alternative approach is to modify the degree of coupling between the MSP and an optical cavity.[132] Indeed, by placing the MQW structure within an optical metal–metal resonator, where the metal also serves as a Schottky contact to deplete of charge the MQWs, the system can be tuned in and out of the ultra-strong coupling regime, hence producing an energy shift of the polariton branches (Sec. IV). This shift produces a change in reflectance of the metamaterial that can be used as a MIR amplitude modulator up to GHz.[132] However, this concept could be difficult to generalize to MSPs due to limited electric field penetration in highly doped semiconductor layers. An alternative approach could be working with tunnel coupled asymmetric quantum wells,[133] where the ISBT energy is submitted to a linear Stark effect.

VIII. OUTLOOK

In this Perspectives paper, we have overviewed the status of research into MSPs and described the paths we believe the topic is going to follow in the future. A description of the basic physics of MSPs is given, as well as of the interaction of MSPs with optical modes in a cavity and phonons in the crystal lattice, highlighting the extraordinary potential of MSPs in these fields. The potential, pros and cons in MSP-based applications of a selection of semiconductors were also provided, stressing the state of the art and prospects in specific applications of each semiconductor. Finally, the prospects of new studies, physics, and devices based on MSPs were analyzed.

We have found that MSPs provide a platform in which a large variety of physical phenomena can be studied. This is due in part to the large density of electrons usually involved in MSPs that yields the high coupling coefficients between MSPs and either optical modes in a cavity or lattice oscillations in the crystals, which allow reaching the ultra-strong coupling regime. We firmly believe there is large room for the use of MSPs as a platform for studies of fundamental physical phenomena of which several examples have been described in this work.

Also, MSPs are starting to find room in the development of new devices for the emission and detection of light, based on their superradiant nature or due to the fact that they can be strongly and ultrastrongly coupled to cavities so their emission can be tuned down in energy, reaching the always desired range of the THz. We recognize the use of MSPs in devices is still in an early stage, therefore we are confident there lies a brilliant research future in the development of these devices.

Finally, we have explored the material platforms with the highest potential to allow reaching all these goals. Some of the analyzed materials are in a more mature position for MSP-based applications, whereas others are still mostly virgin territory for MSP research. This, quite obviously, is not a drawback, but rather an opportunity for researchers willing to delve in this exciting research topic, which, in our opinion, is ripe to give groundbreaking findings and inventions.

ACKNOWLEDGMENTS

This work was funded by the Spanish Ministry of Science and Innovation under Project No. PID2020-114796RB-C21, by the Agence Nationale de la Recherche (COLECTOR project, Grant No. ANR-19-CE30-0032-01) and by the ENS-Thales Chair. Solution of the Schrödinger equation in the structures presented in this paper was partially realized using the Aestimo solver.[134] The authors would like to acknowledge Professor E. Tournié, Professor Y. Dumont, Dr. Y. Cordier, and Dr. B. Damilano for their useful remarks.

AUTHOR DECLARATIONS

Conflict of Interest

The authors have no conflicts to disclose.

Author Contributions

M. Montes Bajo: Conceptualization (equal); Data curation (equal); Formal analysis (equal); Funding acquisition (equal); Investigation

(equal); Methodology (equal); Project administration (equal); Resources (equal); Software (equal); Supervision (equal); Validation (equal); Visualization (equal); Writing – original draft (lead); Writing – review & editing (lead). **J.-M. Chauveau:** Data curation (equal); Formal analysis (equal); Funding acquisition (equal); Investigation (equal); Methodology (equal); Project administration (equal); Resources (equal); Supervision (equal); Validation (equal); Visualization (equal); Writing – original draft (equal); Writing – review & editing (equal). **A. Vasanelli:** Data curation (equal); Formal analysis (equal); Funding acquisition (equal); Investigation (equal); Methodology (equal); Project administration (equal); Resources (equal); Software (equal); Supervision (equal); Validation (equal); Visualization (equal); Writing – original draft (equal); Writing – review & editing (lead). **A. Delteil:** Data curation (equal); Formal analysis (equal); Investigation (equal); Methodology (equal); Software (equal); Validation (equal); Visualization (equal); Writing – original draft (equal); Writing – review & editing (equal). **Y. Todorov:** Data curation (equal); Formal analysis (equal); Funding acquisition (equal); Investigation (equal); Methodology (equal); Project administration (equal); Resources (equal); Software (equal); Supervision (equal); Validation (equal); Visualization (equal); Writing – review & editing (equal). **C. Sirtori:** Data curation (equal); Formal analysis (equal); Funding acquisition (equal); Investigation (equal); Methodology (equal); Project administration (equal); Resources (equal); Software (equal); Supervision (equal); Validation (equal); Visualization (equal); Writing – original draft (equal); Writing – review & editing (equal). **A. Hierro:** Conceptualization (lead); Data curation (equal); Formal analysis (equal); Funding acquisition (equal); Investigation (equal); Methodology (equal); Project administration (equal); Resources (equal); Software (equal); Supervision (equal); Validation (equal); Visualization (equal); Writing – original draft (lead); Writing – review & editing (lead).

DATA AVAILABILITY

The data that support the findings of this study are available from the corresponding author upon reasonable request.

REFERENCES

[1]M. Helm, in *Semiconductors and Semimetals*, edited by H. C. Liu and F. Capasso (Elsevier, 1999), Vol. 62, pp. 1–99.
[2]T. Ando, A. B. Fowler, and F. Stern, "Electronic properties of two-dimensional systems," Rev. Mod. Phys. **54**(2), 437–672 (1982).
[3]H. Schneider and H. C. Liu, *Quantum Well Infrared Photodetectors: Physics and Applications*, 2007th ed. (Springer, 2014).
[4]J. Faist, *Quantum Cascade Lasers*, Reprint ed. (Oxford University Press, Oxford, 2018).
[5]A. Kamgar, P. Kneschaurek, G. Dorda, and J. F. Koch, "Resonance spectroscopy of electronic levels in a surface accumulation layer," Phys. Rev. Lett. **32**(22), 1251–1254 (1974).
[6]Z. Schlesinger, J. C. M. Hwang, and S. J. Allen, "Subband-Landau-level coupling in a two-dimensional electron gas," Phys. Rev. Lett. **50**(26), 2098–2101 (1983).
[7]L. C. West and S. J. Eglash, "First observation of an extremely large-dipole infrared transition within the conduction band of a GaAs quantum well," Appl. Phys. Lett. **46**(12), 1156–1158 (1985).
[8]A. Delga, in *Mid-Infrared Optoelectronics*, edited by E. Tournié and L. Cerutti (Woodhead Publishing, 2020), pp. 337–377.
[9]J. Faist, F. Capasso, D. L. Sivco, C. Sirtori, A. L. Hutchinson, and A. Y. Cho, "Quantum cascade laser," Science **264**(5158), 553–556 (1994).
[10]C. Sirtori, P. Kruck, S. Barbieri, P. Collot, J. Nagle, M. Beck, J. Faist, and U. Oesterle, "GaAs/$Al_xGa_{1-x}As$ quantum cascade lasers," Appl. Phys. Lett. **73**(24), 3486–3488 (1998).
[11]A. Delteil, A. Vasanelli, Y. Todorov, C. Feuillet Palma, M. Renaudat St-Jean, G. Beaudoin, I. Sagnes, and C. Sirtori, "Charge-induced coherence between intersubband plasmons in a quantum structure," Phys. Rev. Lett. **109**(24), 246808 (2012).
[12]B. Askenazi, A. Vasanelli, A. Delteil, Y. Todorov, L. C. Andreani, G. Beaudoin, I. Sagnes, and C. Sirtori, "Ultra-strong light–matter coupling for designer Reststrahlen band," New J. Phys. **16**(4), 043029 (2014).
[13]A. Vasanelli, Y. Todorov, and C. Sirtori, "Ultra-strong light–matter coupling and superradiance using dense electron gases," C. R. Phys. **17**(8), 861–873 (2016).
[14]A. Vasanelli, S. Huppert, A. Haky, T. Laurent, Y. Todorov, and C. Sirtori, "Semiconductor quantum plasmonics," Phys. Rev. Lett. **125**(18), 187401 (2020).
[15]S. Ribeiro, A. Vasanelli, Y. Todorov, and C. Sirtori, "Quantum theory of multisubband plasmon–phonon coupling," Photonics **7**(1), 19 (2020).
[16]W. J. Pasek, C. Deimert, P. Goulain, J.-M. Manceau, R. Colombelli, and Z. R. Wasilewski, "Multisubband plasmons: Beyond the parabolicity in the semiclassical model," Phys. Rev. B **106**(11), 115303 (2022).
[17]B. Askenazi, A. Vasanelli, Y. Todorov, E. Sakat, J.-J. Greffet, G. Beaudoin, I. Sagnes, and C. Sirtori, "Midinfrared ultrastrong light–matter coupling for THz thermal emission," ACS Photonics **4**(10), 2550–2555 (2017).
[18]C. Deimert, P. Goulain, J.-M. Manceau, W. Pasek, T. Yoon, A. Bousseksou, N. Y. Kim, R. Colombelli, and Z. R. Wasilewski, "Realization of harmonic oscillator arrays with graded semiconductor quantum wells," Phys. Rev. Lett. **125**(9), 097403 (2020).
[19]M. Geiser, F. Castellano, G. Scalari, M. Beck, L. Nevou, and J. Faist, "Ultrastrong coupling regime and plasmon polaritons in parabolic semiconductor quantum wells," Phys. Rev. Lett. **108**(10), 106402 (2012).
[20]T. Laurent, Y. Todorov, A. Vasanelli, A. Delteil, C. Sirtori, I. Sagnes, and G. Beaudoin, "Superradiant emission from a collective excitation in a semiconductor," Phys. Rev. Lett. **115**(18), 187402 (2015).
[21]M. Montes Bajo, J. Tamayo-Arriola, M. Hugues, J. M. Ulloa, N. Le Biavan, R. Peretti, F. H. Julien, J. Faist, J.-M. Chauveau, and A. Hierro, "Multisubband plasmons in doped ZnO quantum wells," Phys. Rev. Appl. **10**(2), 024005 (2018).
[22]A. Hierro, M. Montes Bajo, M. Ferraro, J. Tamayo-Arriola, N. Le Biavan, M. Hugues, J. M. Ulloa, M. Giudici, J.-M. Chauveau, and P. Genevet, "Optical phase transition in semiconductor quantum metamaterials," Phys. Rev. Lett. **123**(11), 117401 (2019).
[23]F. Alpeggiani and L. C. Andreani, "Semiclassical theory of multisubband plasmons: Nonlocal electrodynamics and radiative effects," Phys. Rev. B **90**(11), 115311 (2014).
[24]S. J. Allen, D. C. Tsui, and B. Vinter, "On the absorption of infrared radiation by electrons in semiconductor inversion layers," Solid State Commun. **88**(11), 939–942 (1993).
[25]S. Vassant, J.-P. Hugonin, F. Marquier, and J.-J. Greffet, "Berreman mode and epsilon near zero mode," Opt. Express **20**(21), 23971–23977 (2012).
[26]S. Campione, I. Brener, and F. Marquier, "Theory of epsilon-near-zero modes in ultrathin films," Phys. Rev. B **91**(12), 121408 (2015).
[27]M. Załużny, "On the influence of the depolarization field on the intersubband absorption in thin semiconductor films," Phys. Status Solidi (B) **123**(1), K57–K61 (1984).
[28]J. Li and C. Z. Ning, "Induced transparency by intersubband plasmon coupling in a quantum well," Phys. Rev. Lett. **93**(8), 087402 (2004).
[29]H. C. Liu, C. Y. Song, Z. R. Wasilewski, A. J. SpringThorpe, J. C. Cao, C. Dharma-wardana, G. C. Aers, D. J. Lockwood, and J. A. Gupta, "Coupled electron-phonon modes in optically pumped resonant intersubband lasers," Phys. Rev. Lett. **90**(7), 077402 (2003).
[30]S. Butscher, J. Förstner, I. Waldmüller, and A. Knorr, "Polaron signatures in the line shape of semiconductor;intersubband transitions: Quantum kinetics of

the electron–phonon interaction," Phys. Status Solidi (B) **241**(11), R49–R51 (2004).
[31]S. Butscher and A. Knorr, "Occurrence of intersubband polaronic repellons in a two-dimensional electron Gas," Phys. Rev. Lett. **97**(19), 197401 (2006).
[32]S. De Liberato and C. Ciuti, "Quantum theory of intersubband polarons," Phys. Rev. B **85**(12), 125302 (2012).
[33]Y. Todorov and C. Sirtori, "Intersubband polaritons in the electrical dipole gauge," Phys. Rev. B **85**(4), 045304 (2012).
[34]Y. Todorov, A. M. Andrews, R. Colombelli, S. De Liberato, C. Ciuti, P. Klang, G. Strasser, and C. Sirtori, "Ultrastrong light-matter coupling regime with polariton dots," Phys. Rev. Lett. **105**(19), 196402 (2010).
[35]P. Nataf and C. Ciuti, "Vacuum degeneracy of a circuit QED system in the ultrastrong coupling regime," Phys. Rev. Lett. **104**(2), 023601 (2010).
[36]M. Kardar and R. Golestanian, "The 'friction' of vacuum, and other fluctuation-induced forces," Rev. Mod. Phys. **71**(4), 1233–1245 (1999).
[37]R. Ferreira and G. Bastard, "Evaluation of some scattering times for electrons in unbiased and biased single- and multiple-quantum-well structures," Phys. Rev. B **40**(2), 1074–1086 (1989).
[38]M. Schubert, *Infrared Ellipsometry on Semiconductor Layer Structures Phonons, Plasmons, and Polaritons* (Springer, Berlin, New York, 2004).
[39]J. B. Khurgin, G. Sun, L. R. Friedman, and R. A. Soref, "Comparative analysis of optically pumped intersubband lasers and intersubband Raman oscillators," J. Appl. Phys. **78**(12), 7398–7400 (1995).
[40]C. Ciuti, G. Bastard, and I. Carusotto, "Quantum vacuum properties of the intersubband cavity polariton field," Phys. Rev. B **72**(11), 115303 (2005).
[41]A. Frisk Kockum, A. Miranowicz, S. De Liberato, S. Savasta, and F. Nori, "Ultrastrong coupling between light and matter," Nat. Rev. Phys. **1**(1), 19–40 (2019).
[42]P. Forn-Díaz, L. Lamata, E. Rico, J. Kono, and E. Solano, "Ultrastrong coupling regimes of light-matter interaction," Rev. Mod. Phys. **91**(2), 025005 (2019).
[43]D. Dini, R. Köhler, A. Tredicucci, G. Biasiol, and L. Sorba, "Microcavity polariton splitting of intersubband transitions," Phys. Rev. Lett. **90**(11), 116401 (2003).
[44]L. Sapienza, A. Vasanelli, R. Colombelli, C. Ciuti, Y. Chassagneux, C. Manquest, U. Gennser, and C. Sirtori, "Electrically injected cavity polaritons," Phys. Rev. Lett. **100**(13), 136806 (2008).
[45]G. Günter, A. A. Anappara, J. Hees, A. Sell, G. Biasiol, L. Sorba, S. De Liberato, C. Ciuti, A. Tredicucci, A. Leitenstorfer, and R. Huber, "Sub-cycle switch-on of ultrastrong light–matter interaction," Nature **458**(7235), 178–181 (2009).
[46]P. Jouy, A. Vasanelli, Y. Todorov, A. Delteil, G. Biasiol, L. Sorba, and C. Sirtori, "Transition from strong to ultrastrong coupling regime in mid-infrared metal-dielectric-metal cavities," Appl. Phys. Lett. **98**(23), 231114 (2011).
[47]Y. Todorov, A. M. Andrews, I. Sagnes, R. Colombelli, P. Klang, G. Strasser, and C. Sirtori, "Strong light-matter coupling in subwavelength metal-dielectric microcavities at terahertz frequencies," Phys. Rev. Lett. **102**(18), 186402 (2009).
[48]J. Casanova, G. Romero, I. Lizuain, J. J. García-Ripoll, and E. Solano, "Deep strong coupling regime of the Jaynes-Cummings model," Phys. Rev. Lett. **105**(26), 263603 (2010).
[49]S. Christopoulos, G. B. H. von Högersthal, A. J. D. Grundy, P. G. Lagoudakis, A. V. Kavokin, J. J. Baumberg, G. Christmann, R. Butté, E. Feltin, J.-F. Carlin, and N. Grandjean, "Room-temperature polariton lasing in semiconductor microcavities," Phys. Rev. Lett. **98**(12), 126405 (2007).
[50]O. Jamadi, F. Reveret, P. Disseix, F. Medard, J. Leymarie, A. Moreau, D. Solnyshkov, C. Deparis, M. Leroux, E. Cambril, S. Bouchoule, J. Zuniga-Perez, and G. Malpuech, "Edge-emitting polariton laser and amplifier based on a ZnO waveguide," Light Sci. Appl. **7**(1), 82 (2018).
[51]F. Boeuf, R. André, R. Romestain, L. Si Dang, E. Péronne, J. F. Lampin, D. Hulin, and A. Alexandrou, "Evidence of polariton stimulation in semiconductor microcavities," Phys. Rev. B **62**(4), R2279–R2282 (2000).
[52]S. De Liberato and C. Ciuti, "Stimulated scattering and lasing of intersubband cavity polaritons," Phys. Rev. Lett. **102**(13), 136403 (2009).
[53]R. Colombelli and J.-M. Manceau, "Perspectives for intersubband polariton lasers," Phys. Rev. X **5**(1), 011031 (2015).
[54]A. Delteil, A. Vasanelli, P. Jouy, D. Barate, J. C. Moreno, R. Teissier, A. N. Baranov, and C. Sirtori, "Optical phonon scattering of cavity polaritons in an electroluminescent device," Phys. Rev. B **83**(8), 081404 (2011).
[55]J.-M. Manceau, N.-L. Tran, G. Biasiol, T. Laurent, I. Sagnes, G. Beaudoin, S. De Liberato, I. Carusotto, and R. Colombelli, "Resonant intersubband polariton-LO phonon scattering in an optically pumped polaritonic device," Appl. Phys. Lett. **112**(19), 191106 (2018).
[56]M. Knorr, J. M. Manceau, J. Mornhinweg, J. Nespolo, G. Biasiol, N. L. Tran, M. Malerba, P. Goulain, X. Lafosse, M. Jeannin, M. Stefinger, I. Carusotto, C. Lange, R. Colombelli, and R. Huber, "Intersubband polariton-polariton scattering in a dispersive microcavity," Phys. Rev. Lett. **128**(24), 247401 (2022).
[57]D. A. Anderson, N. Apsley, P. Davies, and P. L. Giles, "Compensation in heavily doped n-type InP and GaAs," J. Appl. Phys. **58**(8), 3059–3067 (1985).
[58]P. Bogusławski and J. Bernholc, "Doping properties of C, Si, and Ge impurities in GaN and AlN," Phys. Rev. B **56**(15), 9496–9505 (1997).
[59]S. Brochen, G. Feuillet, J.-L. Santailler, R. Obrecht, M. Lafossas, P. Ferret, J.-M. Chauveau, and J. Pernot, "Non-metal to metal transition in n-type ZnO single crystal materials," J. Appl. Phys. **121**(9), 095704 (2017).
[60]V. Fan Arcara, B. Damilano, G. Feuillet, A. Courville, S. Chenot, and J.-Y. Duboz, "(Ga,In)N/GaN light emitting diodes with a tunnel junction and a rough n-contact layer grown by metalorganic chemical vapor deposition," AIP Adv. **9**(5), 055101 (2019).
[61]S. Washiyama, K. J. Mirrielees, P. Bagheri, J. N. Baker, J.-H. Kim, Q. Guo, R. Kirste, Y. Guan, M. H. Breckenridge, A. J. Klump, P. Reddy, S. Mita, D. L. Irving, R. Collazo, and Z. Sitar, "Self-compensation in heavily Ge doped AlGaN: A comparison to Si doping," Appl. Phys. Lett. **118**(4), 042102 (2021).
[62]W. Götz, N. M. Johnson, C. Chen, H. Liu, C. Kuo, and W. Imler, "Activation energies of Si donors in GaN," Appl. Phys. Lett. **68**(22), 3144–3146 (1996).
[63]B. Borisov, V. Kuryatkov, Y. Kudryavtsev, R. Asomoza, S. Nikishin, D. Y. Song, M. Holtz, and H. Temkin, "Si-doped $Al_xGa_{1-x}N(0.56\leqslant x\leqslant 1)$ layers grown by molecular beam epitaxy with ammonia," Appl. Phys. Lett. **87**(13), 132106 (2005).
[64]R. J. Warburton, K. Weilhammer, J. P. Kotthaus, M. Thomas, and H. Kroemer, "Influence of collective effects on the linewidth of intersubband resonance," Phys. Rev. Lett. **80**(10), 2185–2188 (1998).
[65]S. Nakamura, T. Mukai, and M. Senoh, "Candela-class high-brightness InGaN/AlGaN double-heterostructure blue-light-emitting diodes," Appl. Phys. Lett. **64**, 1687–1689 (1994).
[66]A. Vardi, G. Bahir, F. Guillot, C. Bougerol, E. Monroy, S. E. Schacham, M. Tchernycheva, and F. H. Julien, "Near infrared quantum cascade detector in GaN/AlGaN/AlN heterostructures," Appl. Phys. Lett. **92**(1), 011112 (2008).
[67]A. Ajay, C. B. Lim, D. A. Browne, J. Polaczyński, E. Bellet-Amalric, J. Bleuse, M. I. den Hertog, and E. Monroy, "Effect of doping on the intersubband absorption in Si- and Ge-doped GaN/AlN heterostructures," Nanotechnology **28**(40), 405204 (2017).
[68]P. Quach, S. F. Liu, A. Jollivet, D. Wang, J. Y. Cheng, N. Isac, S. Pirotta, D. Bouville, S. S. Sheng, A. Imran, L. Chen, D. Li, X. T. Zheng, Y. X. Wang, Z. X. Qin, M. Tchernycheva, F. H. Julien, B. Shen, and X. Q. Wang, "A GaN/AlN quantum cascade detector with a broad response from the mid-infrared (4.1 μm) to the visible (550 nm) spectral range," Appl. Phys. Lett. **116**(17), 171102 (2020).
[69]M. Monavarian, J. Xu, M. Khoury, F. Wu, P. De Mierry, P. Vennegues, M. A. Belkin, and J. S. Speck, "Defect tolerance of intersubband transitions in nonpolar GaN/(Al,Ga)N heterostructures: A path toward low-cost and scalable mid- to far-infrared optoelectronics," Phys. Rev. Appl. **16**(5), 054040 (2021).
[70]K. Frei, R. Trejo-Hernández, S. Schütt, L. Kirste, M. Prescher, R. Aidam, S. Müller, P. Waltereit, O. Ambacher, and M. Fiederle, "Investigation of growth parameters for ScAlN-barrier HEMT structures by plasma-assisted MBE," Jpn. J. Appl. Phys. **58**(SC), SC1045 (2019).
[71]A. J. Green, J. K. Gillespie, R. C. Fitch, D. E. Walker, M. Lindquist, A. Crespo, D. Brooks, E. Beam, A. Xie, V. Kumar, J. Jimenez, C. Lee, Y. Cao, K. D. Chabak,

and G. H. Jessen, "ScAlN/GaN high-electron-mobility transistors with 2.4-A/mm current density and 0.67-S/mm transconductance," IEEE Electron Device Lett. **40**(7), 1056–1059 (2019).
[72]P. Wang, D. Wang, B. Wang, S. Mohanty, S. Diez, Y. Wu, Y. Sun, E. Ahmadi, and Z. Mi, "N-polar ScAlN and HEMTs grown by molecular beam epitaxy," Appl. Phys. Lett. **119**(8), 082101 (2021).
[73]I. Gorczyca, H. Teisseyre, T. Suski, N. E. Christensen, and A. Svane, "Structural and electronic properties of wurtzite MgZnO and BeMgZnO alloys and their thermodynamic stability," J. Appl. Phys. **120**(21), 215704 (2016).
[74]J.-M. Chauveau, J. Vives, J. Zuniga-Perez, M. Laügt, M. Teisseire, C. Deparis, C. Morhain, and B. Vinter, "Residual strain in nonpolar a-plane $Zn_{1-x}MgxO$ ($0 < x < 0.55$) and its effect on the band structure of (Zn,Mg)O/ZnO quantum wells," Appl. Phys. Lett. **93**(23), 231911 (2008).
[75]S. Sadofev, S. Kalusniak, P. Schäfer, and F. Henneberger, "Molecular beam epitaxy of n-Zn(Mg)O as a low-damping plasmonic material at telecommunication wavelengths," Appl. Phys. Lett. **102**(18), 181905 (2013).
[76]M. Belmoubarik, K. Ohtani, and H. Ohno, "Intersubband transitions in ZnO multiple quantum wells," Appl. Phys. Lett. **92**(19), 191906 (2008).
[77]N. Le Biavan, M. Hugues, M. Montes Bajo, J. Tamayo-Arriola, A. Jollivet, D. Lefebvre, Y. Cordier, B. Vinter, F.-H. Julien, A. Hierro, and J.-M. Chauveau, "Homoepitaxy of non-polar ZnO/(Zn,Mg)O multi-quantum wells: From a precise growth control to the observation of intersubband transitions," Appl. Phys. Lett. **111**(23), 231903 (2017).
[78]K. Zhao, G. Chen, B.-S. Li, and A. Shen, "Mid-infrared intersubband absorptions in ZnO/ZnMgO multiple quantum wells," Appl. Phys. Lett. **104**(21), 212104 (2014).
[79]B. Hinkov, H. T. Hoang, M. Hugues, J.-M. Chauveau, and G. Strasser, "Etching of m-plane Zn(Mg)O epitaxial films and its impact on surface leakage currents," Semicond. Sci. Technol. **36**(3), 035023 (2021).
[80]A. Jollivet, B. Hinkov, S. Pirotta, H. Hoang, S. Derelle, J. Jaeck, M. Tchernycheva, R. Colombelli, A. Bousseksou, M. Hugues, N. Le Biavan, J. Tamayo-Arriola, M. Montes Bajo, L. Rigutti, A. Hierro, G. Strasser, J. M. Chauveau, and F. H. Julien, "Short infrared wavelength quantum cascade detectors based on m-plane ZnO/ZnMgO quantum wells," Appl. Phys. Lett. **113**(25), 251104 (2018).
[81]B. Meng, B. Hinkov, N. M. L. Biavan, H. T. Hoang, D. Lefebvre, M. Hugues, D. Stark, M. Franckié, A. Torres-Pardo, J. Tamayo-Arriola, M. M. Bajo, A. Hierro, G. Strasser, J. Faist, and J. M. Chauveau, "Terahertz intersubband electroluminescence from nonpolar m-plane ZnO quantum cascade structures," ACS Photonics **8**(1), 343–349 (2021).
[82]N. Grandjean, B. Damilano, S. Dalmasso, M. Leroux, M. Laügt, and J. Massies, "Built-in electric-field effects in wurtzite AlGaN/GaN quantum wells," J. Appl. Phys. **86**(7), 3714–3720 (1999).
[83]C. Morhain, T. Bretagnon, P. Lefebvre, X. Tang, P. Valvin, T. Guillet, B. Gil, T. Taliercio, M. Teisseire-Doninelli, B. Vinter, and C. Deparis, "Internal electric field in wurtzite $ZnO/Zn_{0.78}Mg_{0.22}O$ quantum wells," Phys. Rev. B **72**(24), 241305 (2005).
[84]P. Waltereit, O. Brandt, A. Trampert, H. T. Grahn, J. Menniger, M. Ramsteiner, M. Reiche, and K. H. Ploog, "Nitride semiconductors free of electrostatic fields for efficient white light-emitting diodes," Nature **406**(6798), 865–868 (2000).
[85]T. Wang, "Topical review: Development of overgrown semi-polar GaN for high efficiency green/yellow emission," Semicond. Sci. Technol. **31**(9), 093003 (2016).
[86]J. M. Chauveau, M. Laügt, P. Venneguès, M. Teisseire, B. Lo, C. Deparis, C. Morhain, and B. Vinter, "Non-polar a-plane ZnMgO/ZnO quantum wells grown by molecular beam epitaxy," Semicond. Sci. Technol. **23**(3), 035005 (2008).
[87]P. Dłużewski, J. Z. Domagala, S. Kret, D. Jarosz, M. Kryśko, and H. Teisseyre, "Phase-transition critical thickness of rocksalt $Mg_xZn_{1-x}O$ layers," J. Chem. Phys. **154**(15), 154701 (2021).
[88]I. Gorczyca, M. Wierzbowska, D. Jarosz, J. Z. Domagala, A. Reszka, D. Le Si Dang, F. Donatini, N. E. Christensen, and H. Teisseyre, "Rocksalt ZnMgO alloys for ultraviolet applications: Origin of band-gap fluctuations and direct-indirect transitions," Phys. Rev. B **101**(24), 245202 (2020).
[89]J. Zhang, J. Chen, T. Zhang, D. Gu, L. Shen, L. Wang, H. Xu, and Y. Liu, "Resonant tunneling light emitting diode based on rock-salt ZnO/MgO multiple quantum well," Opt. Mater. **134**, 113232 (2022).
[90]D. J. Paul, "The progress towards terahertz quantum cascade lasers on silicon substrates," Laser Photonics Rev. **4**(5), 610–632 (2010).
[91]D. Sabbagh, J. Schmidt, S. Winnerl, M. Helm, L. Di Gaspare, M. De Seta, M. Virgilio, and M. Ortolani, "Electron dynamics in silicon–germanium terahertz quantum fountain structures," ACS Photonics **3**(3), 403–414 (2016).
[92]T. Grange, D. Stark, G. Scalari, J. Faist, L. Persichetti, L. D. Gaspare, M. D. Seta, M. Ortolani, D. J. Paul, G. Capellini, S. Birner, and M. Virgilio, "Room temperature operation of n-type Ge/SiGe terahertz quantum cascade lasers predicted by non-equilibrium Green's functions," Appl. Phys. Lett. **114**(11), 111102 (2019).
[93]D. Stark, M. Mirza, L. Persichetti, M. Montanari, S. Markmann, M. Beck, T. Grange, S. Birner, M. Virgilio, C. Ciano, M. Ortolani, C. Corley, G. Capellini, L. D. Gaspare, M. D. Seta, D. J. Paul, J. Faist, and G. Scalari, "THz intersubband electroluminescence from n-type Ge/SiGe quantum cascade structures," Appl. Phys. Lett. **118**(10), 101101 (2021).
[94]L. Persichetti, M. Montanari, C. Ciano, L. Di Gaspare, M. Ortolani, L. Baldassarre, M. Zoellner, S. Mukherjee, O. Moutanabbir, G. Capellini, M. Virgilio, and M. De Seta, "Intersubband transition engineering in the conduction band of asymmetric coupled Ge/SiGe quantum wells," Crystals **10**(3), 179 (2020).
[95]C. Xu, J. Kouvetakis, and J. Menéndez, "Doping dependence of the optical dielectric function in n-type germanium," J. Appl. Phys. **125**(8), 085704 (2019).
[96]J. E. Ortmann, N. Nookala, Q. He, L. Gao, C. Lin, A. B. Posadas, A. Y. Borisevich, M. A. Belkin, and A. A. Demkov, "Quantum confinement in oxide heterostructures: Room-temperature intersubband absorption in $SrTiO_3$/$LaAlO_3$ multiple quantum wells," ACS Nano **12**(8), 7682–7689 (2018).
[97]M. Bouras, D. Han, S. Cueff, R. Bachelet, and G. Saint-Girons, "Perovskite-oxide based hyperbolic metamaterials," ACS Photonics **6**(7), 1755–1762 (2019).
[98]W. Wunderlich, H. Ohta, and K. Koumoto, "Enhanced effective mass in doped $SrTiO_3$ and related perovskites," Phys. B **404**(16), 2202–2212 (2009).
[99]H. Ohta, K. Sugiura, and K. Koumoto, "Recent progress in oxide thermoelectric materials: P-type $Ca_3Co_4O_9$ and n-type $SrTiO_3^-$," Inorg. Chem. **47**(19), 8429–8436 (2008).
[100]N. Stanojević, J. Radovanović, and N. Vuković, "Calculation of intersubband absorption in n-doped $BaSnO_3$ quantum wells," Opt. Quant. Electron. **55**, 383 (2023).
[101]A. K. Geim and I. V. Grigorieva, "Van der waals heterostructures," Nature **499**(7459), 419–425 (2013).
[102]Y. Shimazaki, I. Schwartz, K. Watanabe, T. Taniguchi, M. Kroner, and A. Imamoğlu, "Strongly correlated electrons and hybrid excitons in a moiré heterostructure," Nature **580**(7804), 472–477 (2020).
[103]P. Schmidt, F. Vialla, S. Latini, M. Massicotte, K.-J. Tielrooij, S. Mastel, G. Navickaite, M. Danovich, D. A. Ruiz-Tijerina, C. Yelgel, V. Fal'ko, K. S. Thygesen, R. Hillenbrand, and F. H. L. Koppens, "Nano-imaging of intersubband transitions in van der Waals quantum wells," Nat. Nanotechnol. **13**(11), 1035–1041 (2018).
[104]A. Allain and A. Kis, "Electron and hole mobilities in single-layer WSe_2," ACS Nano **8**(7), 7180–7185 (2014).
[105]M. Sidler, P. Back, O. Cotlet, A. Srivastava, T. Fink, M. Kroner, E. Demler, and A. Imamoglu, "Fermi polaron-polaritons in charge-tunable atomically thin semiconductors," Nat. Phys. **13**(3), 255–261 (2017).
[106]S. Huppert, A. Vasanelli, T. Laurent, Y. Todorov, G. Pegolotti, G. Beaudoin, I. Sagnes, and C. Sirtori, "Radiatively broadened incandescent sources," ACS Photonics **2**(12), 1663–1668 (2015).
[107]S. Huppert, A. Vasanelli, G. Pegolotti, Y. Todorov, and C. Sirtori, "Strong and ultrastrong coupling with free-space radiation," Phys. Rev. B **94**(15), 155418 (2016).

[108]R. H. Dicke, "Coherence in spontaneous radiation processes," Phys. Rev. **93**(1), 99–110 (1954).
[109]K. Cong, Q. Zhang, Y. Wang, G. T. Noe, A. Belyanin, and J. Kono, "'Dicke superradiance in solids," J. Opt. Soc. Am. B **33**(7), C80–C101 (2016).
[110]N. Skribanowitz, I. P. Herman, J. C. MacGillivray, and M. S. Feld, "Observation of Dicke superradiance in optically pumped HF gas," Phys. Rev. Lett. **30**(8), 309–312 (1973).
[111]A. Goban, C.-L. Hung, J. D. Hood, S.-P. Yu, J. A. Muniz, O. Painter, and H. J. Kimble, "Superradiance for atoms trapped along a photonic crystal waveguide," Phys. Rev. Lett. **115**(6), 063601 (2015).
[112]M. Scheibner, T. Schmidt, L. Worschech, A. Forchel, G. Bacher, T. Passow, and D. Hommel, "Superradiance of quantum dots," Nat. Phys. **3**(2), 106–110 (2007).
[113]H. Fidder, J. Knoester, and D. A. Wiersma, "Superradiant emission and optical dephasing in J-aggregates," Chem. Phys. Lett. **171**(5–6), 529–536 (1990).
[114]A. F. van Loo, A. Fedorov, K. Lalumière, B. C. Sanders, A. Blais, and A. Wallraff, "Photon-mediated interactions between distant artificial atoms," Science **342**(6165), 1494–1496 (2013).
[115]Q. Zhang, T. Arikawa, E. Kato, J. L. Reno, W. Pan, J. D. Watson, M. J. Manfra, M. A. Zudov, M. Tokman, M. Erukhimova, A. Belyanin, and J. Kono, "Superradiant decay of cyclotron resonance of two-dimensional electron gases," Phys. Rev. Lett. **113**(4), 047601 (2014).
[116]G. Pegolotti, A. Vasanelli, Y. Todorov, and C. Sirtori, "Quantum model of coupled intersubband plasmons," Phys. Rev. B **90**(3), 035305 (2014).
[117]A. Vasanelli, Y. Todorov, B. Dailly, S. Cosme, D. Gacemi, A. Haky, I. Sagnes, and C. Sirtori, "Semiconductor quantum plasmons for high frequency thermal emission," Nanophotonics **10**(1), 607–615 (2021).
[118]J.-J. Greffet, R. Carminati, K. Joulain, J.-P. Mulet, S. Mainguy, and Y. Chen, "Coherent emission of light by thermal sources," Nature **416**(6876), 61–64 (2002).
[119]E. Gornik and D. C. Tsui, "Voltage-tunable far-infrared emission from Si inversion layers," Phys. Rev. Lett. **37**(21), 1425–1428 (1976).
[120]T. Laurent, Y. Todorov, A. Vasanelli, I. Sagnes, G. Beaudoin, and C. Sirtori, "Electrical excitation of superradiant intersubband plasmons," Appl. Phys. Lett. **107**(24), 241112 (2015).
[121]L. Sapienza, A. Vasanelli, C. Ciuti, C. Manquest, C. Sirtori, R. Colombelli, and U. Gennser, "Photovoltaic probe of cavity polaritons in a quantum cascade structure," Appl. Phys. Lett. **90**(20), 201101 (2007).
[122]M. Lagrée, M. Jeannin, G. Quinchard, O. Ouznali, A. Evirgen, V. Trinité, R. Colombelli, and A. Delga, "Direct polariton-to-electron tunneling in quantum cascade detectors operating in the strong light-matter coupling regime," Phys. Rev. Appl. **17**(4), 044021 (2022).
[123]A. Haky, Semiconductor Quantum Plasmonics (Université Paris Sciences & Lettres, 2022).
[124]M. Załużny and C. Nalewajko, "Coupling of infrared radiation to intersubband transitions in multiple quantum wells: The effective-medium approach," Phys. Rev. B **59**(20), 13043–13053 (1999).
[125]M. Montes Bajo, J. Tamayo-Arriola, N. Le Biavan, J. M. Ulloa, P. Vennéguès, D. Lefebvre, M. Hugues, J.-M. Chauveau, and A. Hierro, "Breaking the intersubband selection rules for absorption with ZnO quantum wells: Light polarization sensitivity under normal incidence," Phys. Rev. Appl. **10**(3), 034022 (2018).
[126]T. Taliercio and P. Biagioni, "Semiconductor infrared plasmonics," Nanophotonics **8**(6), 949–990 (2019).
[127]S. A. Mann, N. Nookala, S. C. Johnson, M. Cotrufo, A. Mekawy, J. F. Klem, I. Brener, M. B. Raschke, A. Alù, and M. A. Belkin, "Ultrafast optical switching and power limiting in intersubband polaritonic metasurfaces," Optica **8**(5), 606 (2021).
[128]M. Jeannin, J.-M. Manceau, and R. Colombelli, "Unified description of saturation and bistability of intersubband transitions in the weak and strong light-matter coupling regimes," Phys. Rev. Lett. **127**(18), 187401 (2021).
[129]S. Luin, V. Pellegrini, F. Beltram, X. Marcadet, and C. Sirtori, "Interplay between disorder and intersubband collective excitations in the two-dimensional electron gas," Phys. Rev. B **64**(4), 041306 (2001).
[130]V. Berger, N. Vodjdani, D. Delacourt, and J. P. Schnell, "Room-temperature quantum well infrared modulator using a Schottky diode," Appl. Phys. Lett. **68**(14), 1904–1906 (1996).
[131]A. Lupu, M. Tchernycheva, Y. Kotsar, E. Monroy, and F. H. Julien, "Electroabsorption and refractive index modulation induced by intersubband transitions in GaN/AlN multiple quantum wells," Opt. Express **20**(11), 12541 (2012).
[132]S. Pirotta, N.-L. Tran, A. Jollivet, G. Biasiol, P. Crozat, J.-M. Manceau, A. Bousseksou, and R. Colombelli, "Fast amplitude modulation up to 1.5 GHz of mid-IR free-space beams at room-temperature," Nat. Commun. **12**(1), 799 (2021).
[133]C. Sirtori, F. Capasso, D. L. Sivco, A. L. Hutchinson, and A. Y. Cho, "Resonant stark tuning of second-order susceptibility in coupled quantum wells," Appl. Phys. Lett. **60**(2), 151–153 (1992).
[134]H. Hebal, Z. Koziol, S. B. Lisesivdin, and R. Steed, "General-purpose open-source 1D self-consistent Schrödinger–Poisson solver: Aestimo 1D," Comput. Mater. Sci. **186**, 110015 (2021).